Electronic Supplementary Material (ESI) for Journal of Materials Chemistry C.
This journal is © The Royal Society of Chemistry 2024

Electronic Suplementary Information

Evaluation of vanadium coordination compounds derived from simple acetic acid hydrazide as non-conventional semiconductors

Josipa Sarjanović,[a] Edi Topić,[a] Mirta Rubčić, [a] Lidija Androš Dubraja, [b]

Luka Pavić,* [b] Jana Pisk* [a]

[a]*University of Zagreb, Faculty of Science, Department of Chemistry, Horvatovac 102a, Zagreb, Croatia.*

[b]*Ruđer Bošković Institute, Bijenička cesta 54, Zagreb, Croatia*

**Corresponding authors*

E-mail addresses: jana.pisk@chem.pmf.hr, lpavic@irb.hr

Contents

Scheme S1. Vanadium coordination complexes - synthetic pathways. 5

Scheme S2. Hydrazidato =N–NH–(C=O)– and hydrazonato =N–N=(C–O)– ligand forms and reversible deprotonation 6

Figure S1. IR–ATR ligand spectra H_2L^3 7

Figure S2. DSC curve for the ligand H_2L^3 7

Figure S3. IR–ATR spectra for the complex $(NH_4)[VO_2(L^1)]$ (**1**) 8

Figure S4. IR–ATR spectra for the complex $[VO(L^1)(OMe)(MeOH)]$ (**2**) 8

Figure S5. IR–ATR spectra for the complex $[VO_2(HL^2)]$ (**4**) 9

Figure S6. IR–ATR spectra for the complex $[VO(L^3)(OEt)(H_2O)]$ (**5**) 9

Figure S7. IR–ATR spectra for the complex $[VO_2(HL^3)]_2 \cdot 2H_2O$ (**6**) 10

Figure S8. IR–ATR spectra for the complex $[VO(L^3)(OMe)(MeOH)]$ (**7**) 10

Figure S9. TGA/DSC curve for the complex $(NH_4)[VO_2(L^1)]$ (**1**) 11

Figure S10. TGA/DSC curve for the complex $[VO(L^1)(OMe)(MeOH)]$ (**2**) 11

Figure S11. TGA/DSC curve for the complex $[VO_2(HL^2)]$ 12

Figure S12. TGA/DSC curve for the complex $[VO(L^3)(OEt)(H_2O)]$ (**5**) 12

Figure S13. TGA/DSC curve for the complex $[VO_2(HL^3)]_2 \cdot 2H_2O$ (**6**) 13

Figure S14. TGA/DSC curve for the complex $[VO(L^3)(OMe)(MeOH)]$ (**7**) 13

Table S1. Experimental and crystallographic data for compounds $(NH_4)[VO_2(L^1)]$ (**1**), $[VO(L^1)(OMe)(MeOH)]$ (**2**), $[VO(L^2)(OMe)(MeOH)]\cdot MeOH$ (**3**), $[VO(L^3)(OEt)(H_2O)]$ (**5**), $[VO_2(HL^3)]_2 \cdot 2H_2O$ (**6**), $[VO(L^3)(OMe)(MeOH)]$ (**7**), in this work. 14

Table S2. Selected bond lengths, angles and hydrogen bond parameters in the crystal structure of $[VO(L^2)(OMe)(MeOH)]\cdot MeOH$ (**3**) 16

Figure S15. (a) Supramolecular dimers formed through $R44(14)$ hydrogen bonded motif. Crystal packing in $[VO(L^2)(OMe)(MeOH)]\cdot MeOH$ (**3**) viewed down the: (b) a-axis; (c) b-axis, and (d) c-axis. Non-coordinated methanol molecules are presented in the spacefill style. Hydrogen bonds are highlightes as yellow dashed lines 18

Table S3. Selected bond lengths, angles and hydrogen bond parameters in the crystal structure of $[VO(L^3)(OEt)(H_2O)]$ (**5**) 19

Figure S16. Crystal packing in $[VO(L^3)(OEt)(H_2O)]$ (**5**) viewed down the: (a) *a*-axis; (b) *b*-axis, and (c) *c*-axis. Hydrogen bonds are highlightes as yellow dashed lines. 21

Table S4. Selected bond lengths, angles and hydrogen bond parameters in the crystal structure of $(NH_4)[VO_2(L^1)]$ (**1**) 22

Figure S17. Crystal packing in $(NH_4)[VO_2(L^1)]$ (**1**) viewed down the: (a) *a*-axis; (b) *b*-axis, and (c) *c*-axis. Hydrogen bonds are highlightes as yellow dashed lines. 24

Table S5. Selected bond lengths, angles and hydrogen bond parameters in the crystal structure of $[VO(L^1)(OMe)(MeOH)]$ (**2**) 25

Figure S18. Crystal packing in $[VO(L^1)(OMe)(MeOH)]$ (**2**) viewed down the: (a) *a*-axis; (b) *b*-axis. Hydrogen bonds are highlightes as yellow dashed lines. 27

Table S6. Selected bond lengths, angles and hydrogen bond parameters in the crystal structure of $[VO_2(HL^3)]_2 \cdot 2H_2O$ (**5**) 28

Figure S19. Supramolecular layers formed in formed in *ac*-plane in $[VO_2(HL^3)]_2 \cdot 2H_2O$ (**6**) viewed down the: (a) *a*-axis; (b) *b*-axis, (c) *c*-axis. Hydrogen bonds are highlighted as yellow dashed lines. Hydrogen bonds are highlightes as yellow dashed lines. 30

Figure S20. Crystal packing in $[VO_2(HL^3)]_2 \cdot 2H_2O$ (**6**) viewed down the: (a) *a*-axis; (b) *c*-axis. Crystal water molecules are highlighted in spacefill style. Hydrogen bonds are highlightes as yellow dashed lines. 31

Table S7. Selected bond lengths, angles and hydrogen bond parameters in the crystal structure of $[VO(L^3)(OMe)(MeOH)]$ (**7**) 32

Figure S21. (a) Supramolecular dimers formed through $R2210$ hydrogen bonded motif. Crystal packing in $[VO(L^3)(OMe)(MeOH)]$ (**7**) viewed down the: (b) *a*-axis; (c) *b*-axis, and (d) *c*-axis. Non-coordinated methanol molecules are presented in the spacefill style. Hydrogen bonds are highlightes as yellow dashed lines. 34

Figure S22. Temperature-dependent diffraction patterns of $(NH_4)[VO_2(L^1)]$ (**1**) 35

Figure S23. Temperature-dependent diffraction patterns of $[VO(L^1)(OMe)(MeOH)]$ (**2**) 35

Figure S24. Temperature-dependent diffraction patterns of $[VO_2(HL^2)]$ (**4**) 36

Figure S25. Temperature-dependent diffraction patterns of $[VO(L^3)(OEt)(H_2O)]$ (**5**) 36

Figure S26. Temperature-dependent diffraction patterns of $[VO(L^3)(OMe)(MeOH)]$ (**7**) 37

Figure S27. Temperature dependence of refined molar volume of the $(NH_4)[VO_2(L^1)]$ (**1**) compound, which is calculated as $18Vcell$. Vertical bars represent standard uncertainty. Due to poor crystallinity of the compound, and consequently low diffraction data quality, the molar volume could not be refined precisely, but the overall change across the whole temperature range is insignificant - around 2%. However, above 160 °C the sample converts to another phase with similar unit cell parameters. 37

Figure S28. (Top) Temperature dependence of refined molar volume of the $[VO(L^1)(OMe)(MeOH)]$ (**2**) compound, which is calculated as $14Vcell$ below 160 °C, and $18Vcell$ above it. Standard uncertainties are very low, and not visible in the graph. At low temperatures the molar volume corresponds to the VO(L) moiety ligated with methoxy/methanol ligands. Above 110 °C the change in molar volume corresponds to the loss of two methanol molecules per moiety (ca. 100 $Å^3$ as calculated from methanol crystal structure). (Bottom) Above 160 °C sample probably converts to $[VO_2(HL^1)]$, the same phase observed in high temperature PXRD patterns of $(NH_4)[VO_2(L^1)]$ (**1**). 38

Figure S29. Temperature dependence of refined molar volume of the $[VO_2(HL^2)]$ (**4**) compound, which is calculated as $14Vcell$. Vertical bars represent standard uncertainty. Molar volume increases smoothly across the whole temperature range, and the overall change across the whole temperature range is insignificant - around 4%. Partial amorphization begins at around 180 °C, as evidenced by high uncertainty of molar volume at those temperatures. 39

Figure S30. Temperature dependence of refined molar volume of the $[VO(L^3)(OMe)(MeOH)]$ (**7**) compound, which is calculated as $14Vcell$. Vertical bars represent standard uncertainty. At low temperatures the molar volume corresponds to the VO(L) moiety ligated with methoxy/methanol ligands. Above 60 °C the change in molar volume corresponds to loss of one methanol molecule per moiety (ca. 50 $Å^3$ as calculated from methanol crystal structure). Above 120 °C partial amorphization of the sample prevents precise refinements of molar volume 40

Figure S31. Examples of le Bail refinement on temperature-dependent PXRD data of [VO(L^1)(OMe)(MeOH)] (**2**), at (a) 30 °C using unit cell parameters of [VO(L^1)(OMe)(MeOH)], (b) 140 °C, unit cell parameters of intermediate phase: a = 13.310(3) Å, b = 9.9181(17) Å, c = 8.6416(14) Å, α = 100.751(18)°, β = 108.367(10)°, γ = 101.710(17)°, (c) 200 °C, unit cell parameters of [VO_2(HL^1)], a = 15.2143(15) Å, b = 12.8189(13) Å, c = 9.7818(11) Å, α = 107.074(10)°, β = 93.985(11)°, γ = 93.584(9)°. The refinement results for (c) are similar to high temperature phase of (NH_4)[VO_2(L^1)] results. 41

Figure S32. Example of le Bail refinement on temperature-dependent PXRD data of [VO_2(HL^2)] (**4**), at 30 °C using unit cell parameters of [VO_2(HL^2)] (**4**). 42

Figure S33. Example of le Bail refinement on temperature-dependent PXRD dana of [VO(L^3)(OEt)(H_2O)] (**5**), at 30 °C using cell parameters of [VO(L^3)(OEt)(H_2O)] (**5**). 42

Figure S34. Examples of le Bail refinement on temperature-dependent PXRD data of [VO(L^3)(OMe)(MeOH)] (**7**), at (a) 30 °C using unit cell parameters of [VO(L^3)(OMe)(MeOH)] (**7**), (b) 100 °C, unit cell parameters of high-temperature phase: a = 14.532(3) Å, b = 12.726(3) Å, c = 7.0829(10) Å, α = γ = 90 °, β = 92.019(9)°. 43

Table S8. Tabulated weighted residual (R_{wp}) and unit cell parameters refined by le Bail fit from temperature-dependent PXRD data. 44

Fig S35. Complex impedance spectra for **complex 1** at various temperatures in heating/cooling run. The colored open circles denote experimental values, whereas the solid red line corresponds to the best fit. The corresponding equivalent circuit model is composed of parallel combinations of the resistor (R) and the constant-phase element (CPE), used for fitting the data of individual spectra. 47

Fig S36. Complex impedance spectra for **complex 4** (a,b) and **complex 6** (c), at various temperatures in heating/cooling run. The colored open circles denote experimental values, whereas the solid red line corresponds to the best fit. The corresponding equivalent circuit model is composed of parallel combinations of the resistor (R) and the constant-phase element (CPE), used for fitting the data of individual spectra. 47

Figure S37. Conductivity spectra for mononuclear VO(L^1)(OMe)(MeOH)] sample (complex **2**) in heating (a) and cooling (b) runs, and (c) temperature dependence of DC conductivity (log(σ_{DC}) vs. 1000/T) for both runs (red circle—heating, blue circle—cooling). 48

Figure S38. Conductivity spectra for mononuclear [VO_2(HL^2)] sample (complex **4**) in heating (a) and cooling (b) runs, and (c) temperature dependence of DC conductivity (log(σ_{DC}) vs. 1000/T) for both runs (red circle—heating, blue circle—cooling). 48

Figure S39. Conductivity spectra for mononuclear [VO(L^3)(OMe)(MeOH)] sample (complex **7**) in heating (a) and cooling (b) runs, and (c) temperature dependence of DC conductivity (log(σ_{DC}) vs. 1000/T) for both runs (red circle—heating, blue circle—cooling). 48

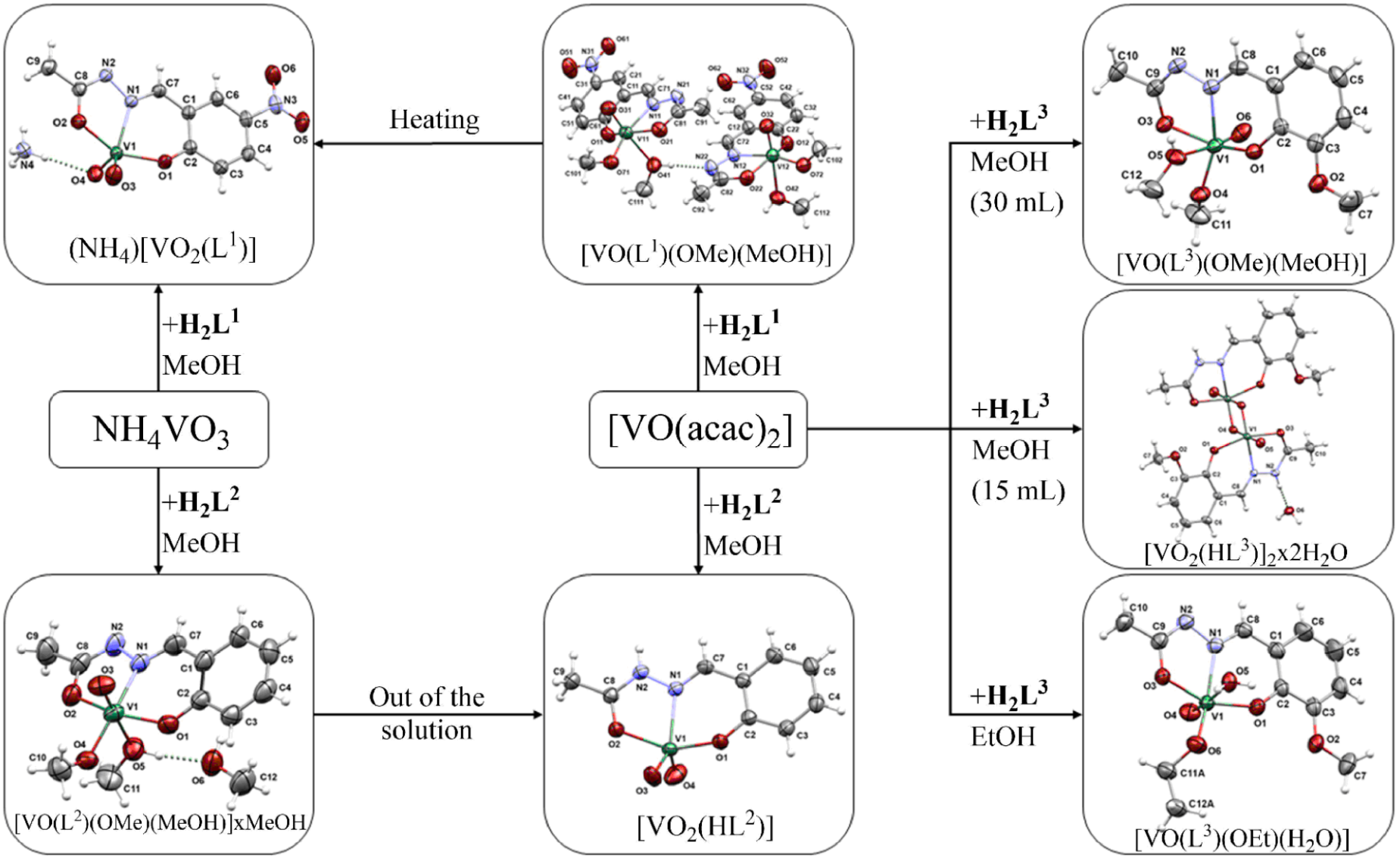

Scheme S1. Vanadium coordination complexes - synthetic pathways.

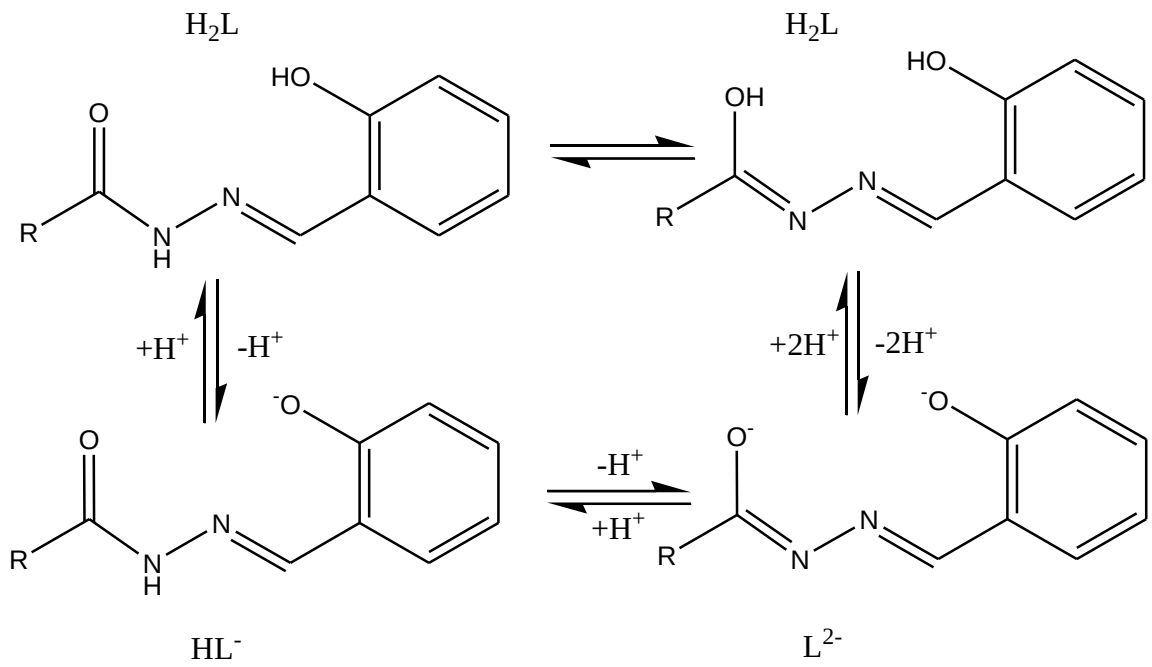

Scheme S2. Hydrazidato =N–NH–(C=O)– and hydrazonato =N–N=(C–O)– ligand forms and reversible deprotonation

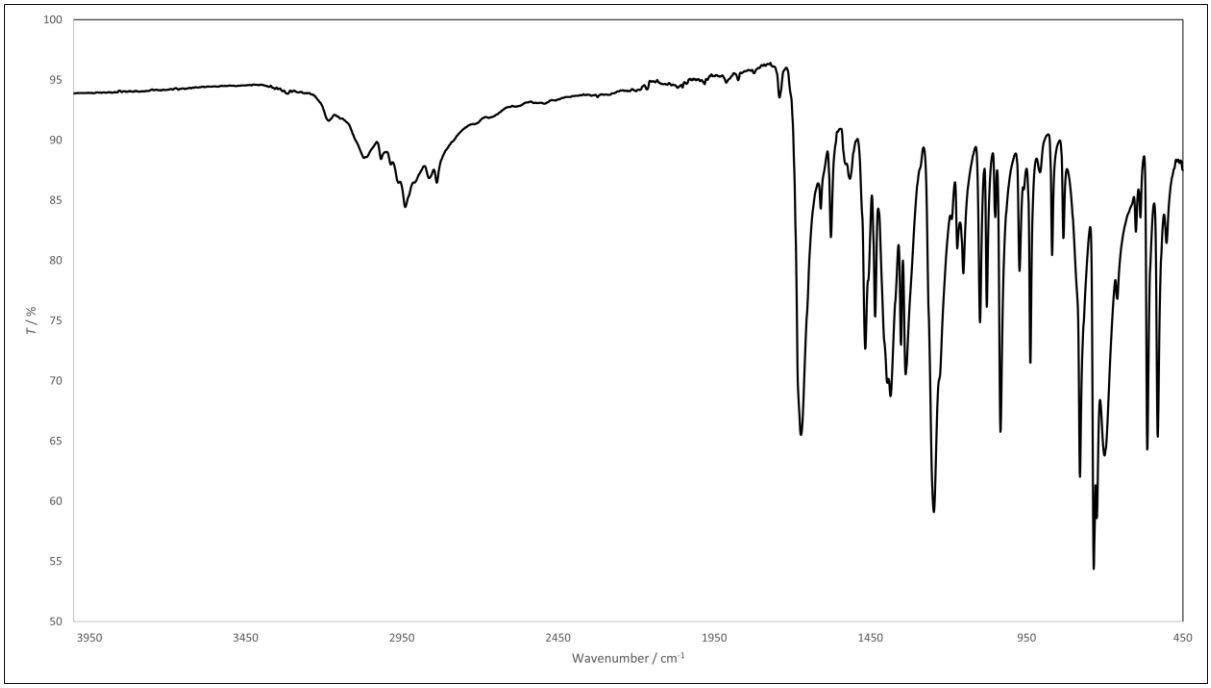

Figure S1. IR–ATR ligand spectra H_2L^3

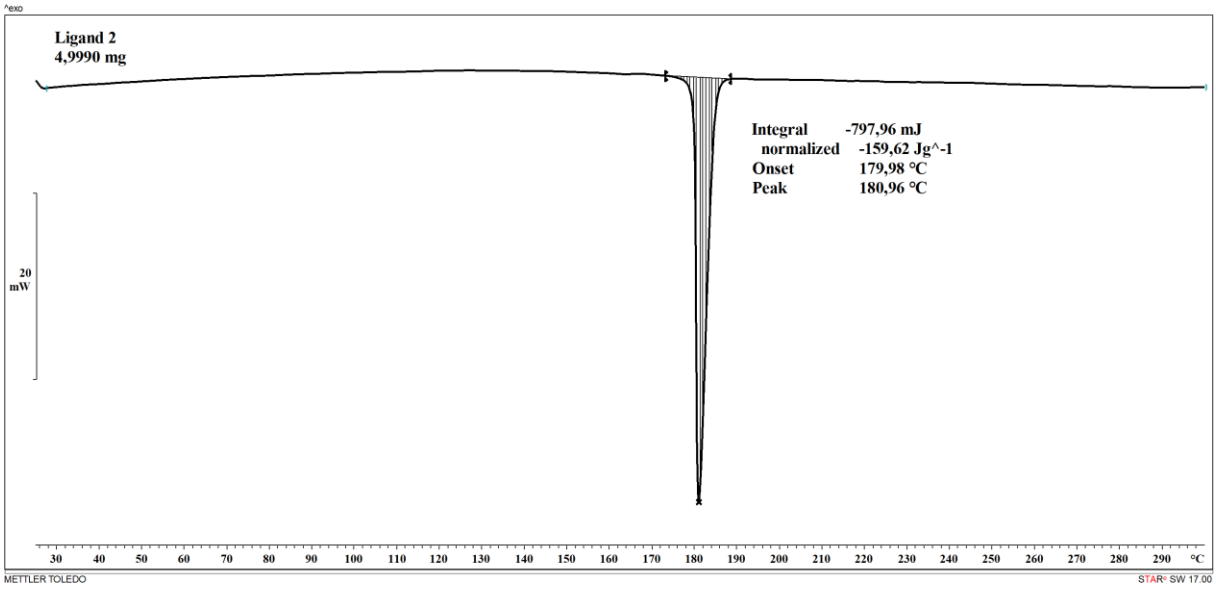

Figure S2. DSC curve for the ligand H_2L^3

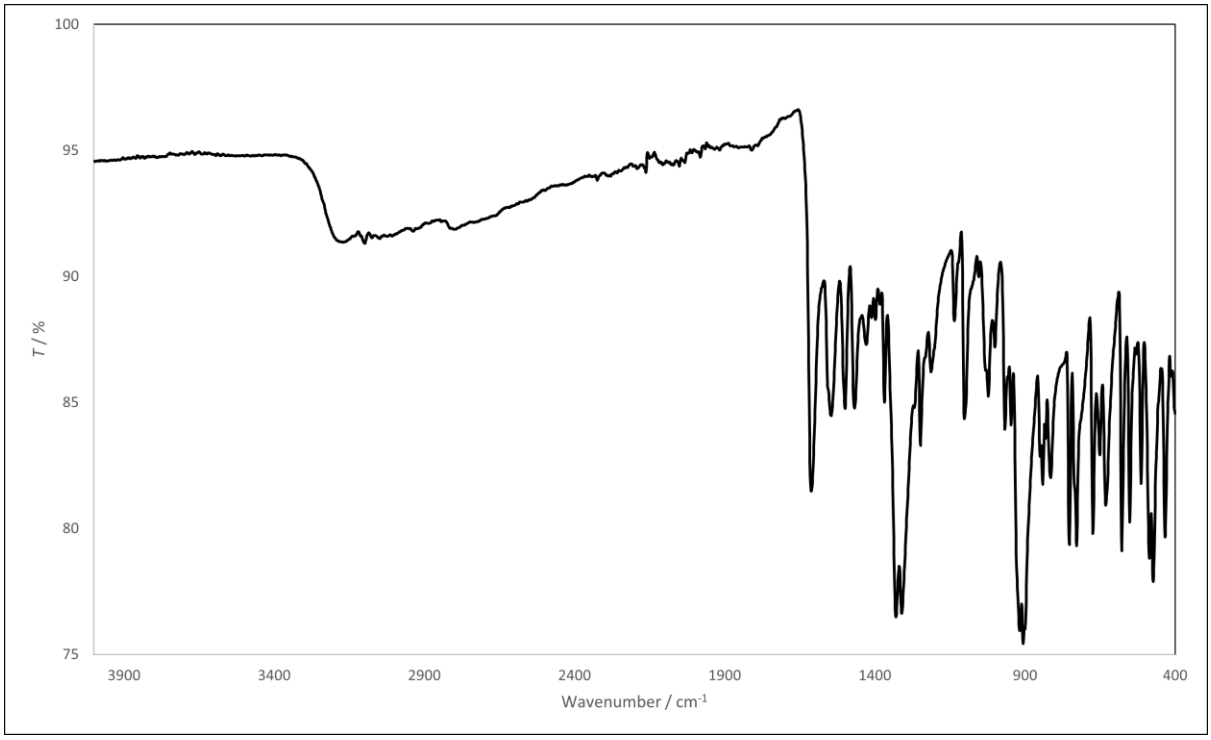

Figure S3. IR–ATR spectra for the complex $(NH_4)[VO_2(L^1)]$ (**1**)

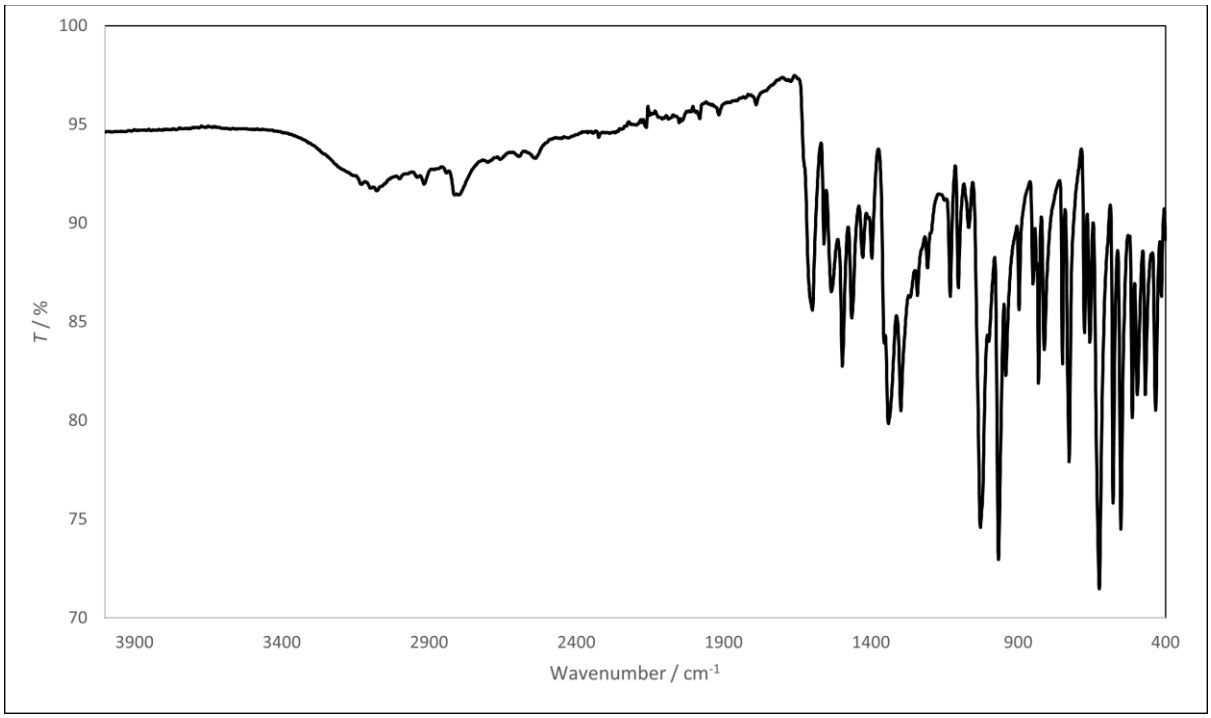

Figure S4. IR–ATR spectra for the complex $[VO(L^1)(OMe)(MeOH)]$ (**2**)

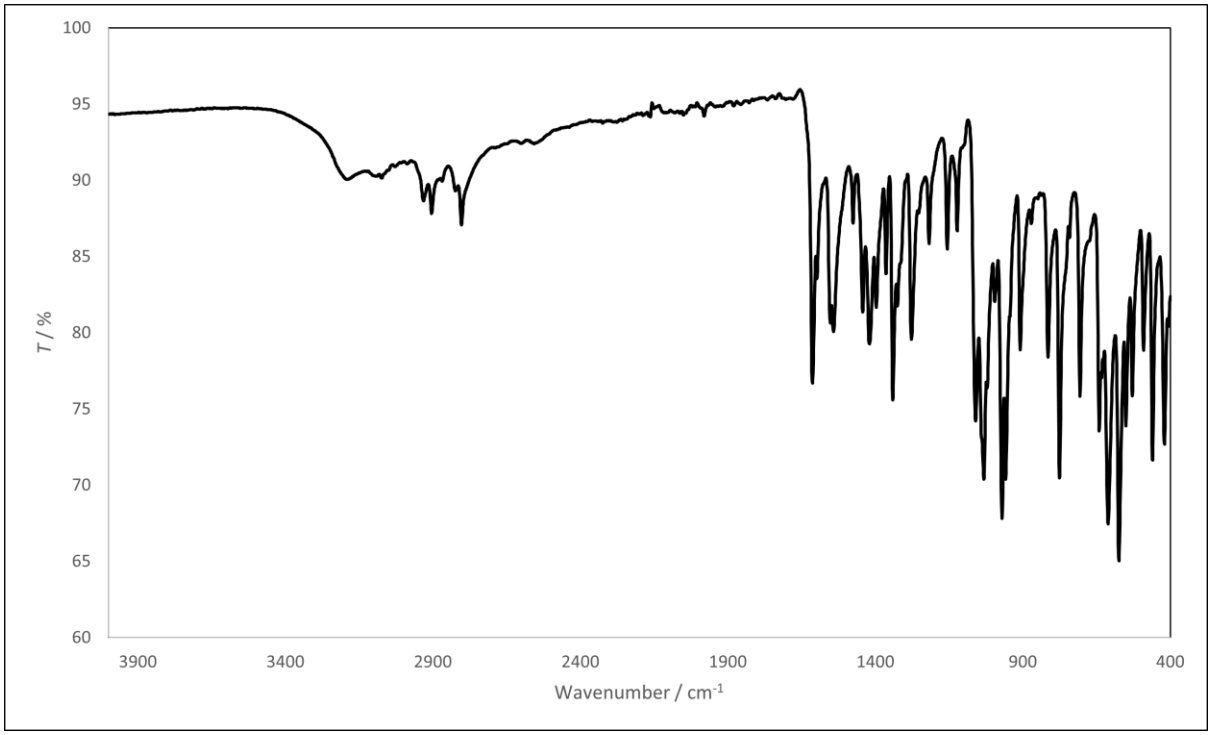

Figure S5. IR–ATR spectra for the complex $[VO_2(HL^2)]$ (**4**)

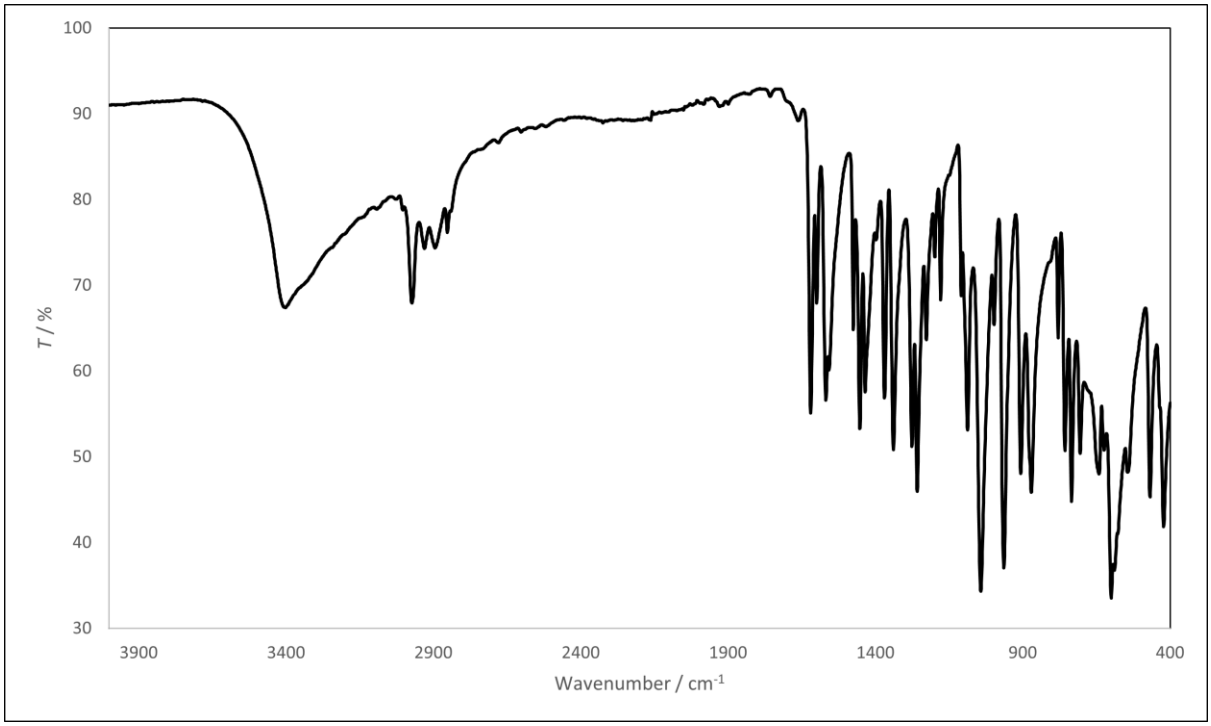

Figure S6. IR–ATR spectra for the complex $[VO(L^3)(OEt)(H_2O)]$ (**5**)

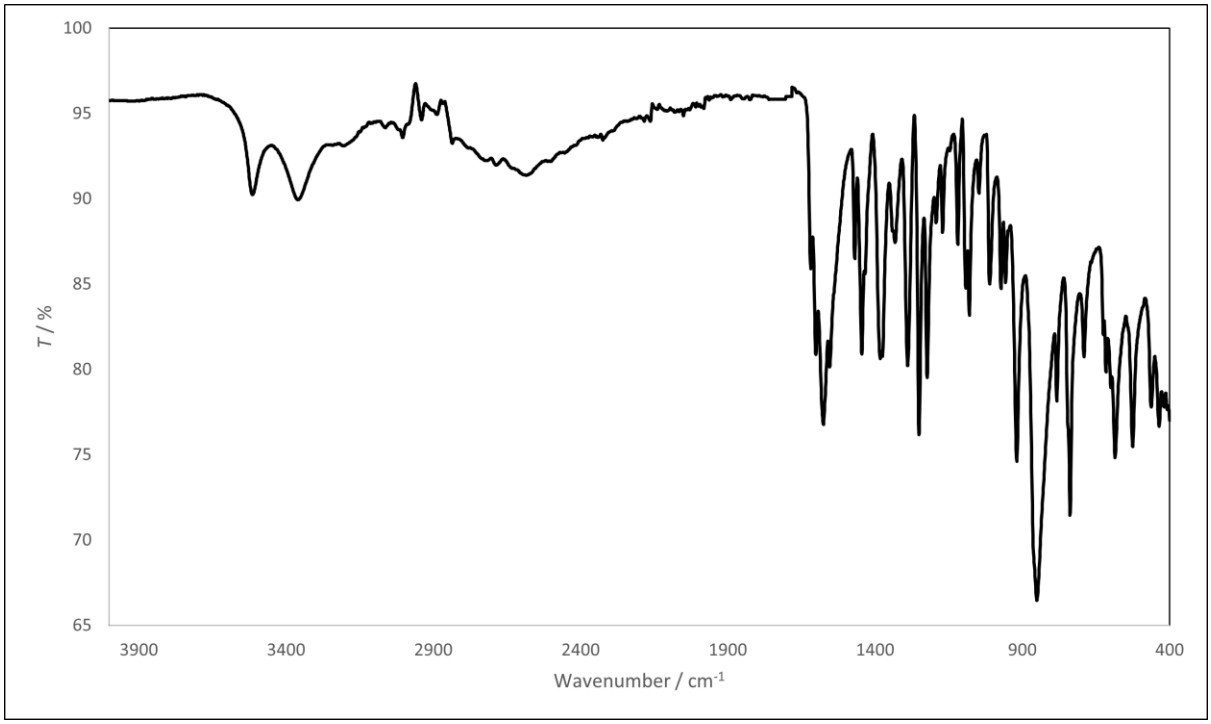

Figure S7. IR–ATR spectra for the complex $[VO_2(HL^3)]_2 \cdot 2H_2O$ (**6**)

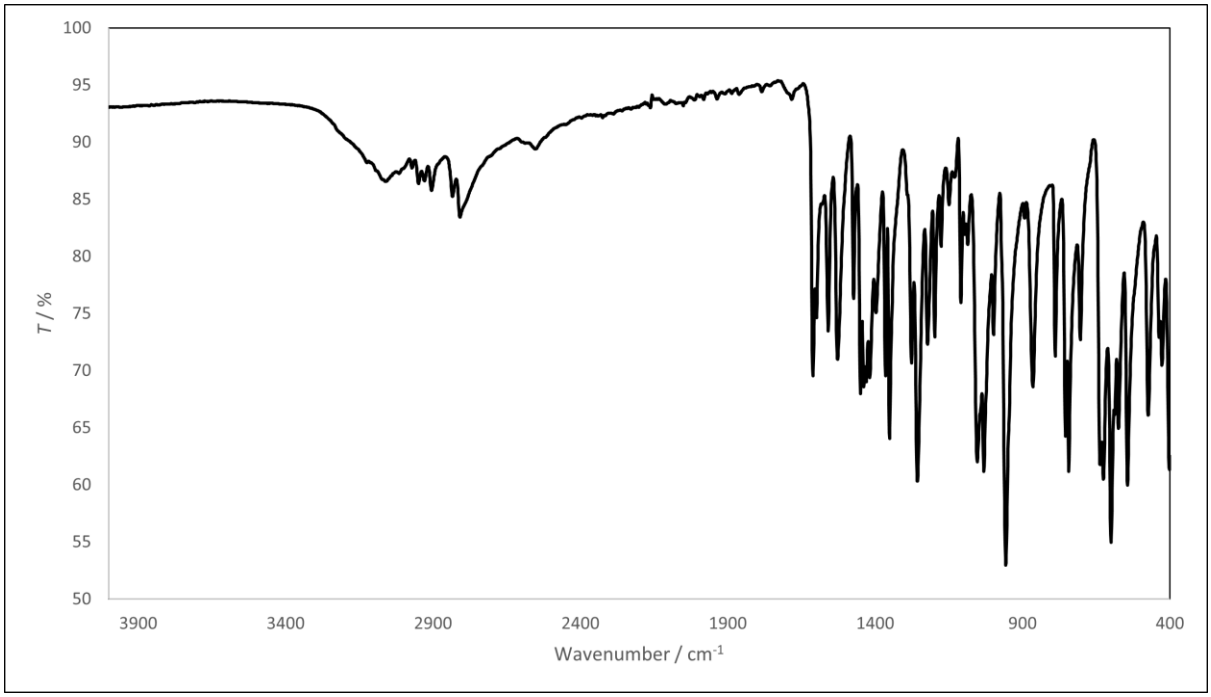

Figure S8. IR–ATR spectra for the complex $[VO(L^3)(OMe)(MeOH)]$ (**7**)

Comparison or IR bands for the obtained vanadium complexes

Vanadium complex	C-O hydrazone	C=N	C-O phenyl	V=O
($(NH_4)[VO_2(L^1)]$]) (**1**)	1330	1612	1248	918, 906
([$VO(L^1)(OMe)(MeOH)$]) (**2**)	1341	1599	1299	967
[$VO_2(HL^2)$] (**4**)	1341	1613	1276	971
[$VO(L^3)(OEt)(H_2O)$] (**5**)	1339	1620	1259	964
[$VO_2(HL^3)]_2 \cdot 2H_2O$ (**6**)	1332	1574	1251	920
[$VO(L_3)(OMe)(MeOH)$] (**7**)	1351	1611	1256	957

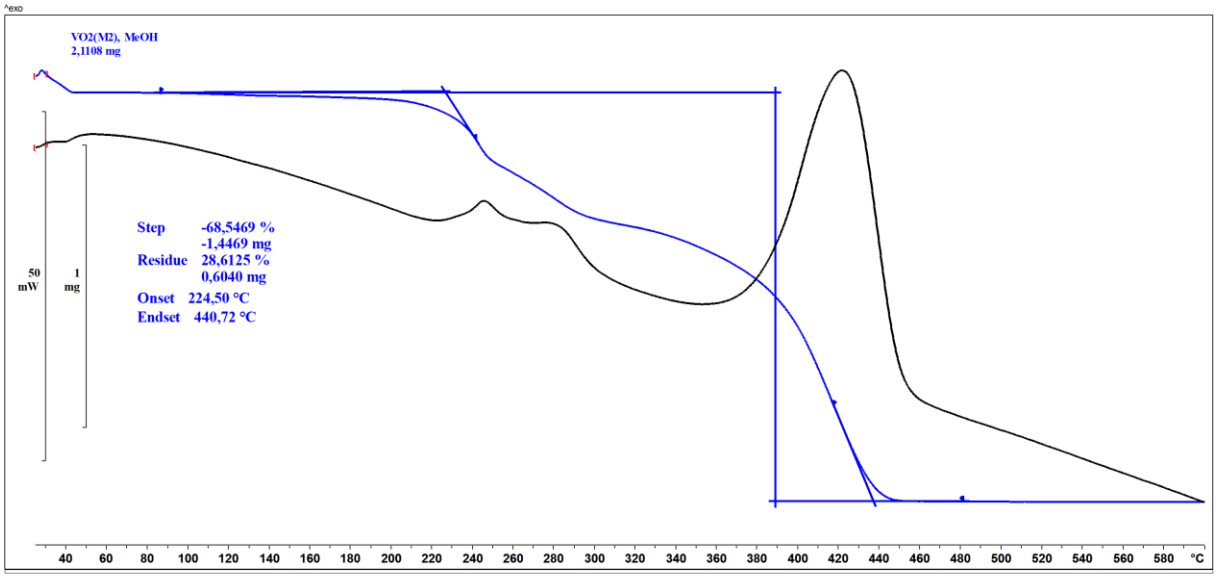

Figure S9. TGA/DSC curve for the complex $(NH_4)[VO_2(L^1)]$ (**1**)

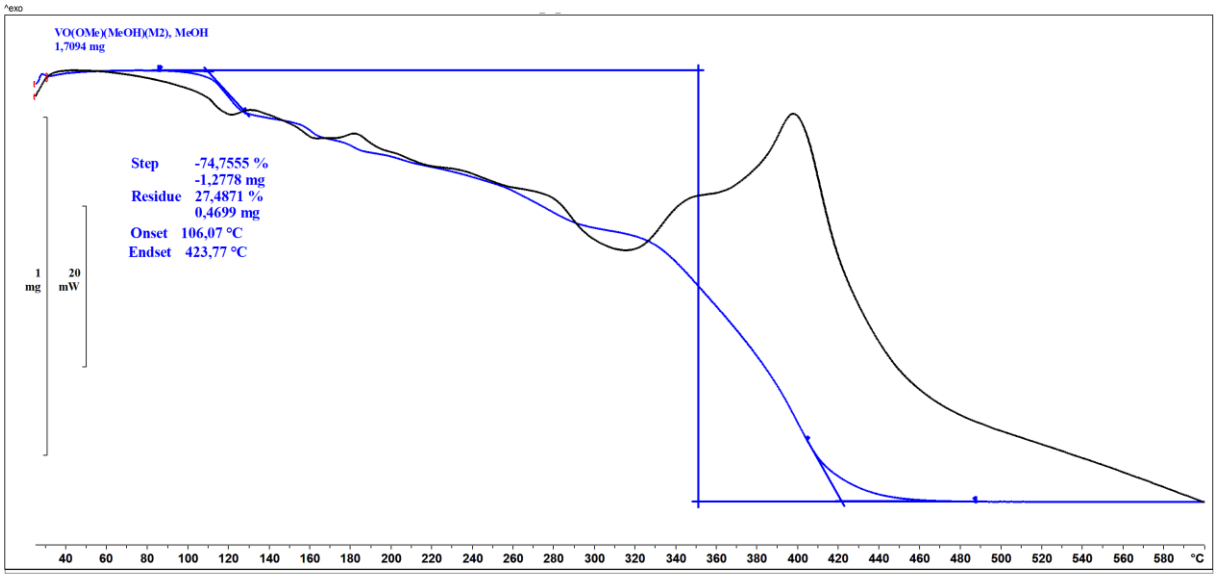

Figure S10. TGA/DSC curve for the complex [$VO(L^1)(OMe)(MeOH)$] (**2**)

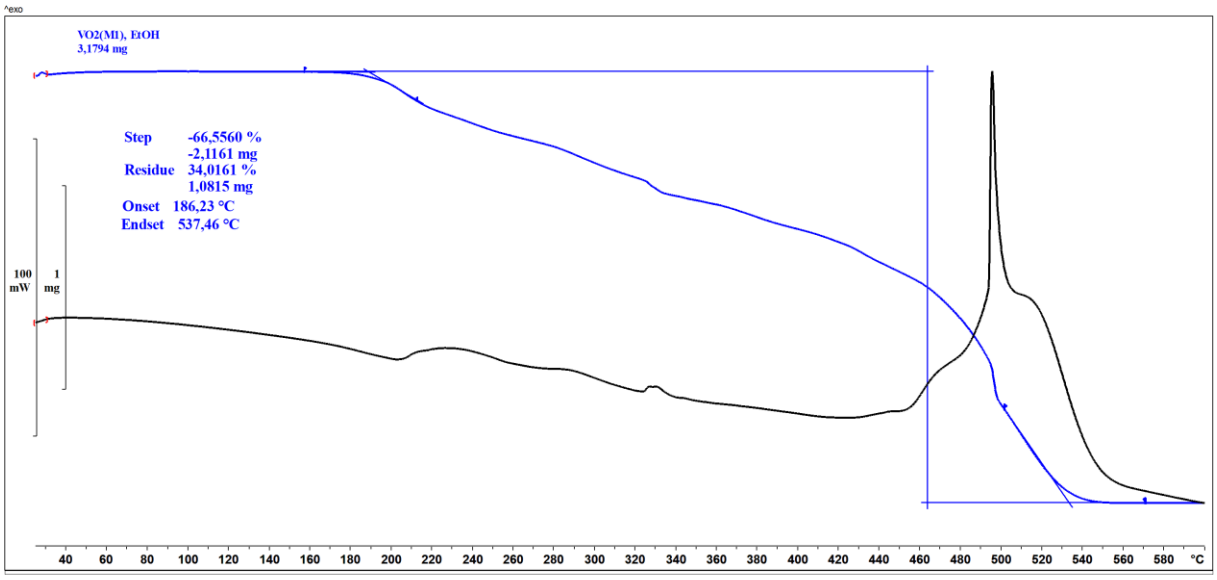

Figure S11. TGA/DSC curve for the complex $[VO_2(HL^2)]$ (**4**)

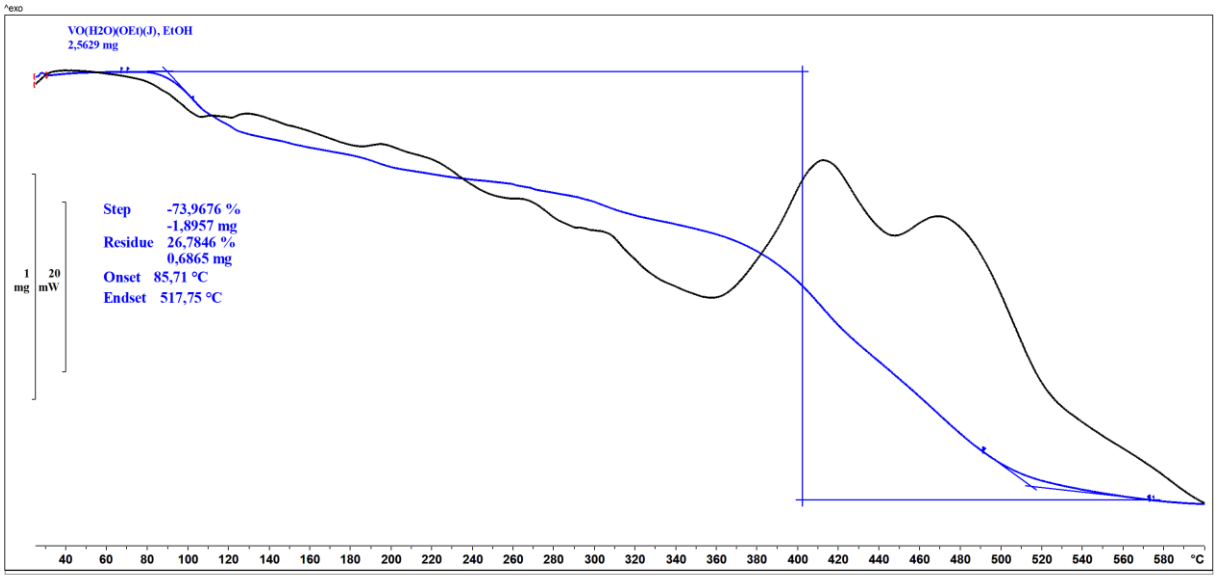

Figure S12. TGA/DSC curve for the complex $[VO(L^3)(OEt)(H_2O)]$ (**5**)

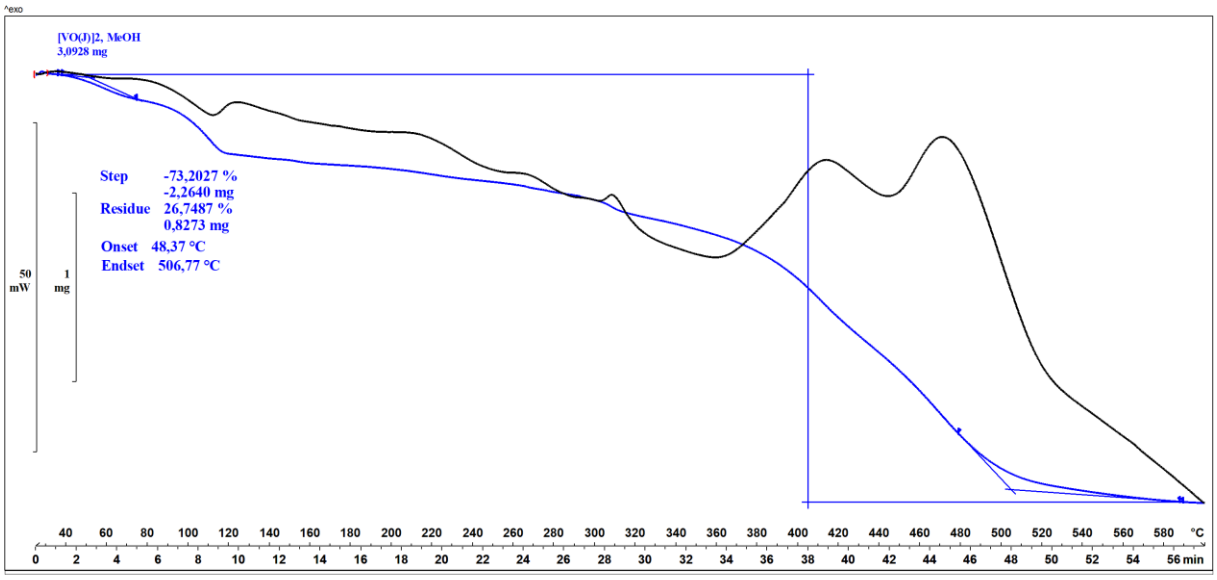

Figure S13. TGA/DSC curve for the complex $[VO_2(HL^3)]_2 \cdot 2H_2O$ (**6**)

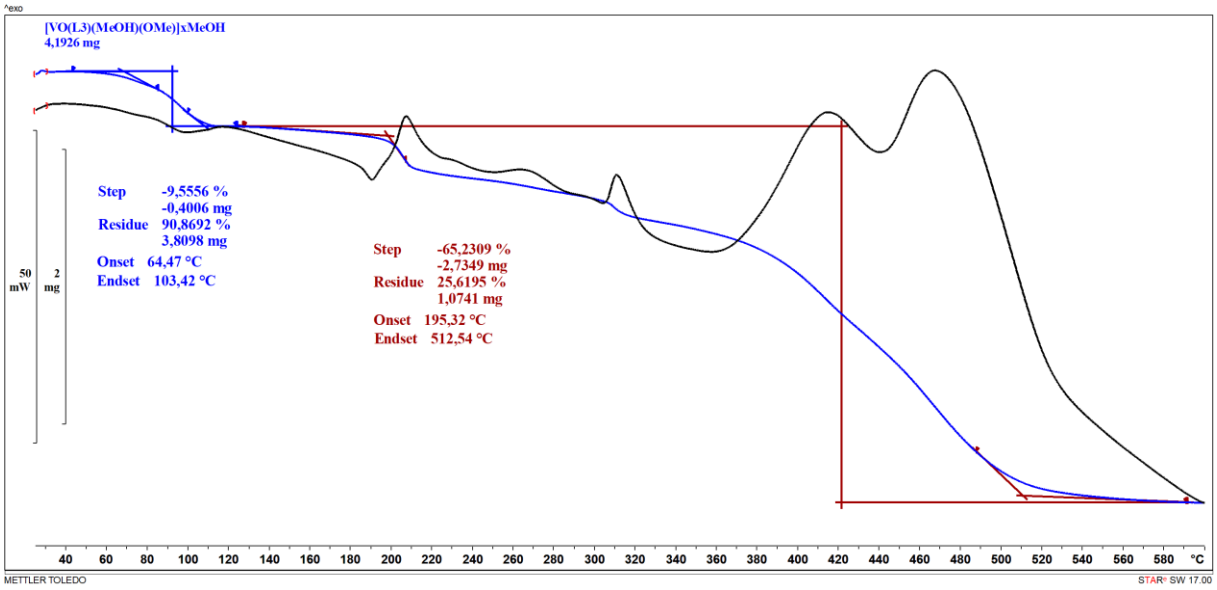

Figure S14. TGA/DSC curve for the complex $[VO(L^3)(OMe)(MeOH)]$ (**7**)

Table S1. Experimental and crystallographic data for compounds $(NH_4)[VO_2(L^1)]$ (**1**), $[VO(L^1)(OMe)(MeOH)]$ (**2**), $[VO(L^2)(OMe)(MeOH)]\cdot MeOH$ (**3**), $[VO(L^3)(OEt)(H_2O)]$ (**5**), $[VO_2(HL^3)]_2\cdot 2H_2O$ (**6**), $[VO(L^3)(OMe)(MeOH)]$ (**7**), in this work.

Identifier	**$[VO(L^2)(OMe)(MeOH)]\cdot MeOH$ (3)**	**$[VO(L^3)(OEt)(H_2O)]$ (5)**	**$(NH_4)[VO_2(L^1)]$ (1)**	**$[VO(L^1)(OMe)(MeOH)]$ (2)**	**$[VO_2(HL^3)]_2\cdot 2H_2O$ (6)**	**$[VO(L^3)(OMe)(MeOH)]$ (7)**
Empirical formula	$C_{12}H_{19}N_2O_6V$	$C_{12}H_{17}N_2O_6V$	$C_9H_{11}N_4O_6V$	$C_{11}H_{14}N_3O_7V$	$C_{20}H_{26}N_4O_{12}V_2$	$C_{12}H_{17}N_2O_6V$
M_r	338.23	336.21	322.16	351.19	616.33	336.21
T/K	293(2)	293(2)	293(2)	293(2)	293(2)	293(2)
Crystal system	triclinic, yellow plate	monoclinic, brown plate	triclinic, yellow prism	triclinic, orange plate	monoclinic, brown plate	monoclinic, brown prism
Space group	$P\,\bar{1}$	$P\,2_1/c$	$P\,\bar{1}$	$P\,\bar{1}$	$P\,2_1/c$	$P\,2_1/c$
a/Å	7.8576(4)	13.5057(4)	7.5057(2)	7.5799(2)	7.41680(6)	8.27200(10)
b/Å	10.2578(5)	10.8764(2)	7.8413(2)	11.0971(4)	21.95187(16)	11.3736(2)
c/Å	10.7080(5)	11.0038(3)	11.1530(3)	17.8091(5)	7.72252(7)	16.1268(3)
α/°	82.970(4)	90	85.945(2)	81.163(2)	90	90
β/°	70.374(5)	109.272(3)	86.982(2)	80.369(2)	96.0455(8)	95.564(2)
γ/°	74.014(4)	90	68.052(3)	89.964(2)	90	90
V/Å^3	781.08(7)	1525.81(7)	607.06(3)	1458.88(8)	1250.331(17)	1510.10(4)
Z	2	4	2	4	2	4
ρ_{calc}/g cm^{-3}	1.438	1.464	1.762	1.599	1.637	1.479
μ/mm^{-1}	5.572	5.705	7.193	6.072	6.903	5.764
F(000)	352	696	328	720	632	696.0
Crystal size/mm^3	0.20×0.12×0.10	0.23×0.19×0.12	0.17×0.14×0.12	0.16×0.09×0.04	0.32×0.14×0.05	0.25 × 0.2 × 0.16
Radiation	Cu Kα (λ = 1.54184Å)					
2Θ range/°	8.772 to 134.97	6.934 to 157.158	7.95 to 155.542	5.096 to 157.81	8.056 to 155.758	9.53 to 155.534
Index ranges	$-9 \le h \le 9$, $-12 \le k \le 12$, $-12 \le l \le 10$	$-17 \le h \le 16$, $-13 \le k \le 13$, $-13 \le l \le 13$	$-9 \le h \le 9$, $-9 \le k \le 9$, $-14 \le l \le 14$	$-9 \le h \le 9$, $-13 \le k \le 14$, $-22 \le l \le 22$	$-9 \le h \le 9$, $-26 \le k \le 27$, $-9 \le l \le 9$	-10 ≤ h ≤ 10, -14 ≤ k ≤ 14, -20 ≤ l ≤ 17
Reflections collected	8429	22137	16601	9655	23889	16020
Independent reflections	2771 [R_{int} = 9.99%, R_{sigma} = 19.88 %]	3220 [R_{int} = 2.97%, R_{sigma} = 5.63 %]	2547 [R_{int} = 1.82%, R_{sigma} = 3.1 %]	9655 [R_{int} = 1.36%]	2664 [R_{int} = 2.03%, R_{sigma} = 4.19 %]	3148 [R_{int} = 2.94%, R_{sigma} = 2.37%]
Data/restraints/parameters	2771/-/199	3220/-/195	2547/-/198	9655/-/412	2664/-/187	3148/-/198
g_1, g_2 in w^a	0.1380, 0	0.0894, 0.8662	0.0459, 0.1599	0.1306, 0.5466	0.0544, 0.2914	0.0545, 0.3155
Goodness–of–fit on F^2, S^b	1.145	1.118	1.102	1.086	1.067	1.079

Final *R* and wR^c values [$I \geq 2\sigma(I)$]	R_1 = 6.99%, wR_2 = 18.76%	R_1 = 5.1%, wR_2 = 14.61%	R_1 = 2.81%, wR_2 = = 7.89%	R_1 = 6.57%, wR_2 = 18.49%	R_1 = 2.86%, wR_2 = 8.33%	R_1 = 0.0312, wR_2 = 0.0881
Final *R* and wR^c values [all data]	R_1 = 12.38%, wR_2 = 26.08%	R_1 = 5.34%, wR_2 = 14.96%	R_1 = 2.91%, wR_2 = 7.96%	R_1 = 7.7%, wR_2 = 20.2%	R_1 = 2.91%, wR_2 = 8.37%	R_1 = 0.0326, wR_2 = 0.0897
Largest diff. peak/hole / e Å^{-3}	0.561/–0.686	0.948/–1.058	0.252/–0.366	0.463/–0.995	0.378/–0.292	0.25/-0.58

[a] $w = 1/[\sigma F_o^2 + (g_1P)^2 + g_2P]$ where $P = (F_o^2 + 2F_c^2)/3$

[b] $S = \{\Sigma[w(F_o^2 - F_c^2)2]/(N_r - N_p)\}^{1/2}$ where N_r = number of independent reflections, N_p = number of refined parameters.

[c] $R = \Sigma||F_o| - |F_c||/\Sigma|F_o|$; $wR = \{\Sigma[w(F_o^2 - F_c^2)2]/\Sigma[w(F_o^2)2]\}^{1/2}$

Table S2. Selected bond lengths, angles and hydrogen bond parameters in the crystal structure of [VO(L^2)(OMe)(MeOH)]·MeOH (**3**)

Atoms	Bond length/Å	Atoms	Bond length/Å	Atoms	Bond length/Å
C1–C2	1.399(9)	O1–C2	1.340(7)	V1–O2	1.950(4)
C1–C6	1.413(10)	O2–C8	1.316(8)	V1–O3	1.590(5)
C1–C7	1.437(9)	O4–C11	1.427(10)	V1–O4	1.784(4)
C2–C3	1.391(9)	O5–C10	1.424(10)	V1–O5	2.262(5)
N1–C7	1.303(9)	O5–H5	0.86(3)		
N1–N2	1.395(8)	V1–N1	2.106(5)		
N2–C8	1.288(9)	V1–O1	1.841(4)		

Atoms	Bond angle/°	Atoms	Bond angle/°	Atoms	Bond angle/°
C2–C1–C6	118.1(6)	V1–N1–N2	116.9(4)	O2–V1–N1	73.94(18)
C2–C1–C7	122.5(6)	N1–N2–C8	108.1(5)	O2–V1–O3	99.7(2)
C6–C1–C7	119.4(6)	V1–O1–C2	132.7(4)	O2–V1–O4	92.94(18)
C1–C2–C3	120.3(6)	V1–O2–C8	118.4(4)	O2–V1–O5	79.8(2)
O1–C2–C1	120.4(6)	V1–O4–C11	129.3(5)	O3–V1–N1	93.6(2)
O1–C2–C3	119.1(5)	C10–O5–H5	107(2)	O3–V1–O4	101.0(2)
C2–C3–C4	119.5(6)	V1–O5–C10	127.5(5)	O3–V1–O5	176.3(2)
C1–C6–C5	121.3(7)	V1–O5–H5	120.9(19)	O4–V1–N1	161.9(2)
N1–C7–C1	122.8(6)	O1–V1–N1	83.28(19)	O4–V1–O5	82.7(2)
O2–C8–C9	116.9(6)	O1–V1–O2	150.6(2)	O5–V1–N1	82.7(2)
O2–C8–N2	122.7(6)	O1–V1–O3	100.0(2)		
N2–N1–C7	116.0(5)	O1–V1–O4	104.38(19)		
V1–N1–C7	126.7(4)	O1–V1–O5	79.2(2)		

D–H···A	D-H	H···A	D···A	∠D–H···A	Symmetry code
O5–H5···O6	0.86(3)	1.79(3)	2.645(7)	172(6)	*x*, *y*, *z*
O6–H6A···N2	0.82	2.02	2.829(7)	169	1–*x*, 1–*y*, 1–*z*
C5–H5A···O2	0.93	2.53	3.458(9)	176	*x*, –1+*y*, *z*

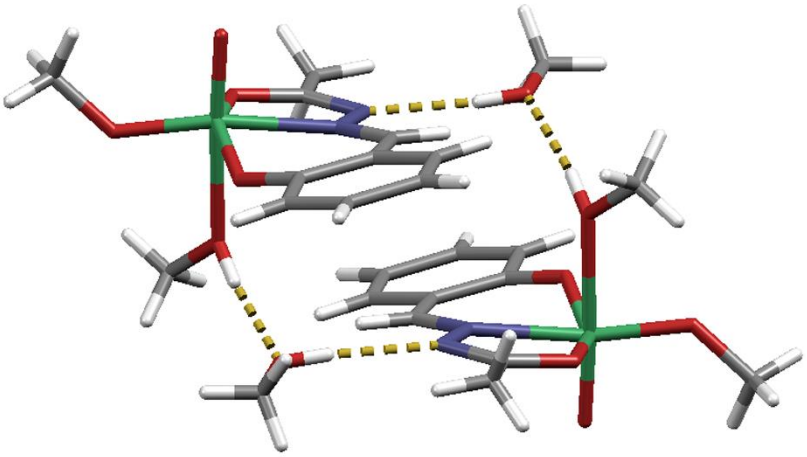

(a)

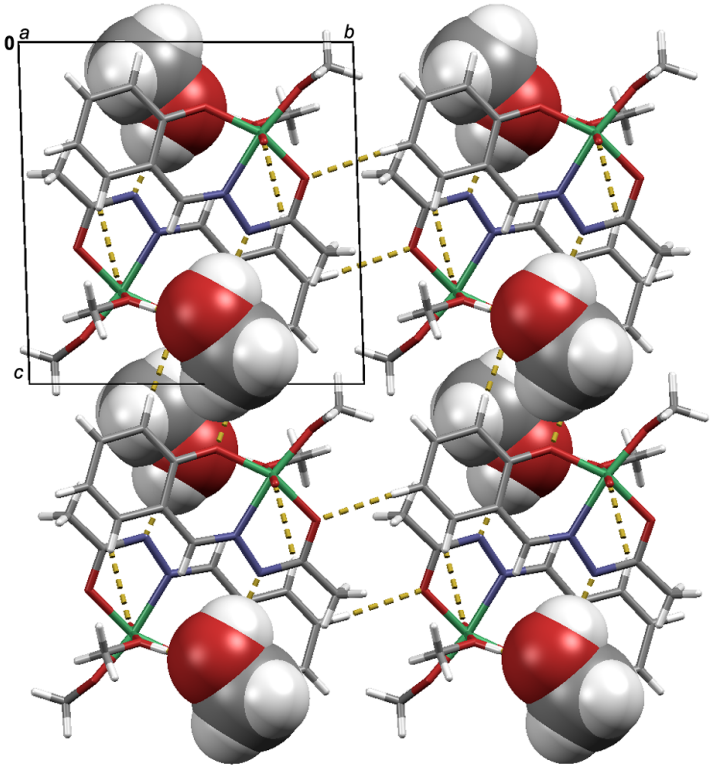

(b)

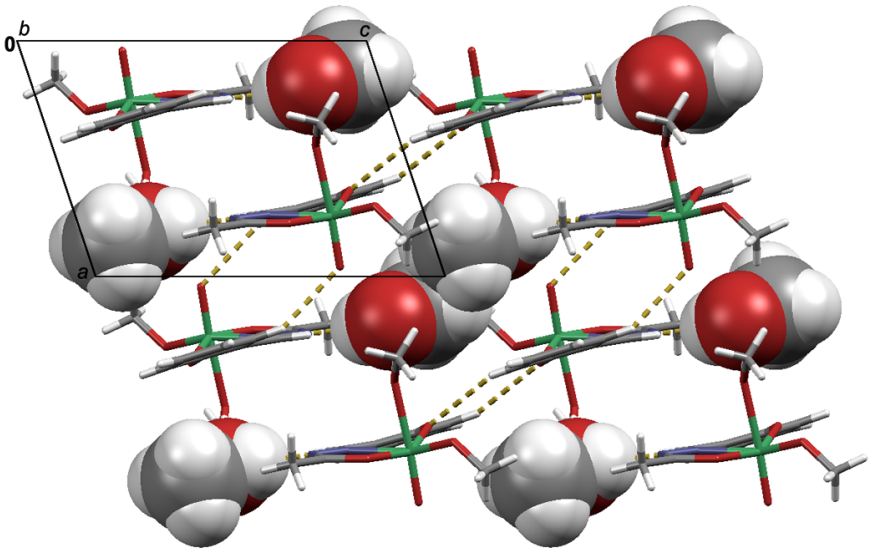

(c)

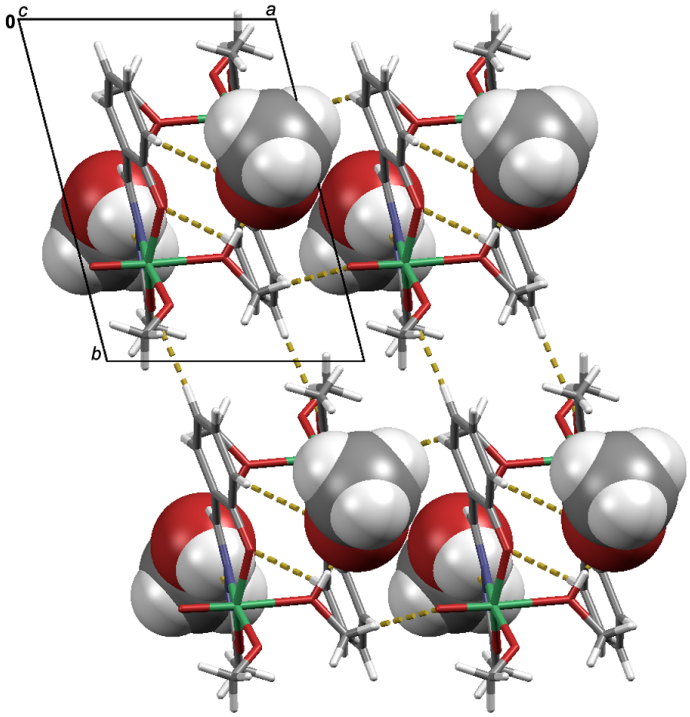

(d)

Figure S15. (a) Supramolecular dimers formed through $R_4^4(14)$ hydrogen bonded motif. Crystal packing in [VO(L^2)(OMe)(MeOH)]·MeOH (**3**) viewed down the: (b) a-axis; (c) b-axis, and (d) c-axis. Non-coordinated methanol molecules are presented in the spacefill style. Hydrogen bonds are highlightes as yellow dashed lines.

Table S3. Selected bond lengths, angles and hydrogen bond parameters in the crystal structure of [VO(L^3)(OEt)(H_2O)] (**5**)

Atoms	Bond length/Å	Atoms	Bond length/Å	Atoms	Bond length/Å
C1–C2	1.395(4)	N2–C9	1.297(4)	V1–N1	2.120(2)
C1–C6	1.408(4)	O1–C2	1.334(3)	V1–O1	1.8456(19)
C1–C8	1.438(4)	O3–C9	1.303(4)	V1–O3	1.9756(19)
C2–C3	1.414(4)	O5–H5A	0.82(3)	V1–O4	1.587(2)
C9–C10	1.489(5)	O5–H5B	0.84(3)	V1–O5	2.296(2)
N1–C8	1.289(3)	O6–C11A	1.474(7)	V1–O6	1.781(2)
N1–N2	1.397(3)	O6–C11B	1.434(9)		

Atoms	Bond angle/°	Atoms	Bond angle/°	Atoms	Bond angle/°
C2–C1–C6	119.7(3)	O6–C11B–C12B	110.0(7)	O1–V1–O4	100.95(10)
C2–C1–C8	121.9(2)	N2–N1–C8	116.2(2)	O1–V1–O5	81.36(8)
C6–C1–C8	118.3(3)	V1–N1–C8	128.19(19)	O1–V1–O6	103.23(9)
C1–C2–C3	119.4(2)	V1–N1–N2	115.40(15)	O3–V1–N1	74.36(8)
O1–C2–C1	122.3(2)	N1–N2–C9	109.3(2)	O3–V1–O4	96.38(10)
O1–C2–C3	118.3(2)	V1–O1–C2	134.83(15)	O3–V1–O5	79.21(7)
C2–C3–C4	119.7(3)	V1–O3–C9	117.49(18)	O3–V1–O6	93.00(9)
O2–C3–C2	115.3(2)	H5A–O5–H5B	106(3)	O4–V1–N1	94.00(10)
C1–C6–C5	120.3(3)	V1–O5–H5A	117(2)	O4–V1–O5	172.97(9)
N1–C8–C1	123.6(2)	V1–O5–H5B	116(2)	O4–V1–O6	101.82(12)
N2–C9–C10	119.3(3)	V1–O6–C11A	125.0(3)	O5–V1–N1	79.58(8)
O3–C9–C10	117.7(3)	V1–O6–C11B	128.5(4)	O5–V1–O6	83.98(10)
O3–C9–N2	122.9(3)	O1–V1–N1	84.05(8)	O6–V1–N1	160.83(11)
O6–C11A–C12A	106.1(5)	O1–V1–O3	153.14(8)		

D–H···A	D-H	H···A	D···A	∠D–H···A	Symmetry code
O5–H5A···N2	0.82(3)	1.99(3)	2.810(3)	178(3)	*x*, 3/2–*y*, 1/2+*z*
O5–H5B···O3	0.84(3)	2.02(3)	2.850(3)	176.9(17)	1–*x*, 1–*y*, 1–*z*
C4–H4···O4	0.93	2.54	3.405(5)	155	2–*x*, 1/2+*y*, 3/2–*z*
C5–H5···O2	0.93	2.49	3.389(4)	163	2–*x*, 1/2+*y*, 3/2–*z*

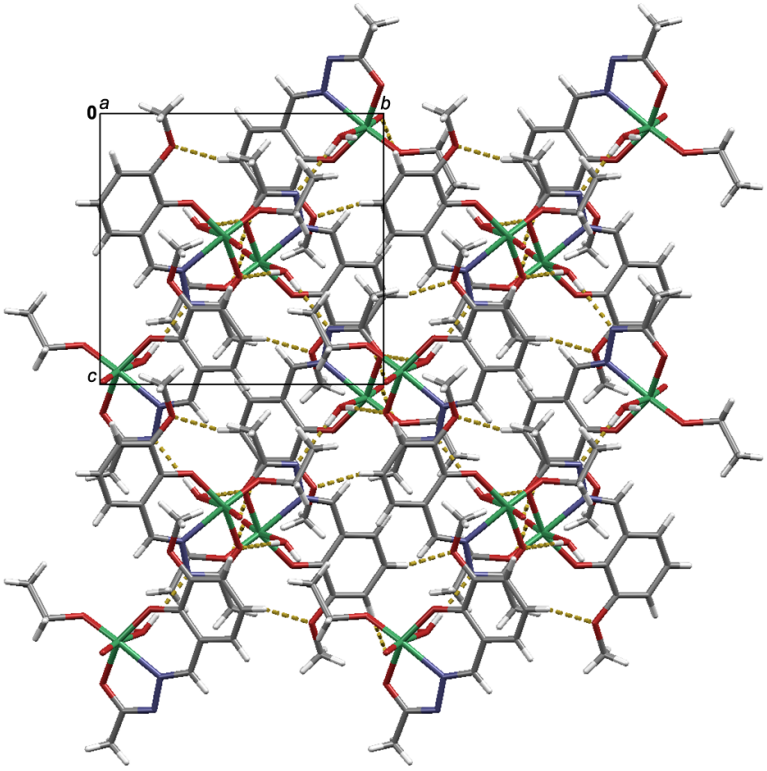

(a)

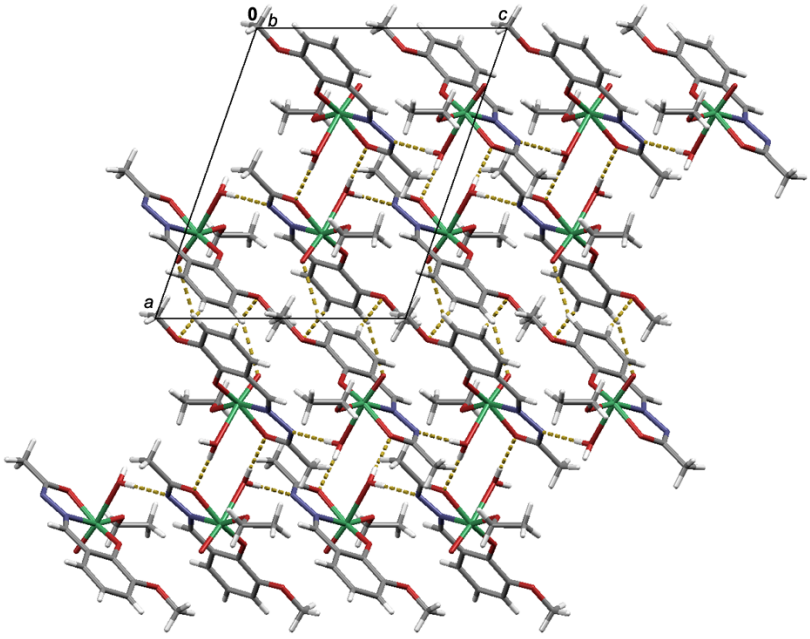

(b)

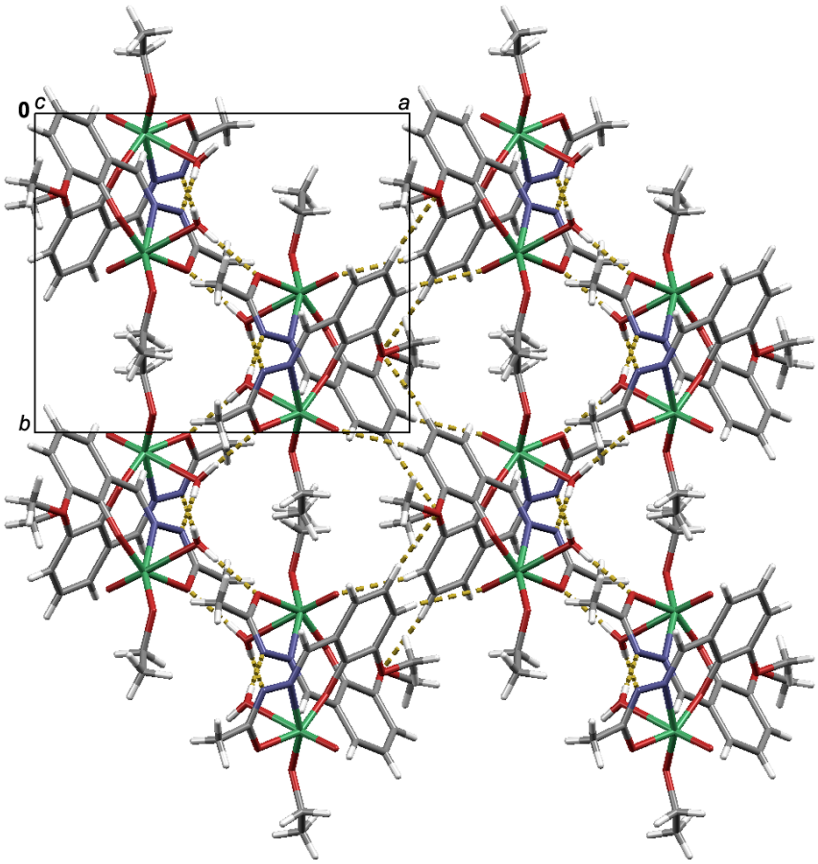

(c)

Figure S16. Crystal packing in [VO(L^3)(OEt)(H_2O)] (**5**) viewed down the: (a) *a*-axis; (b) *b*-axis, and (c) *c*-axis. Hydrogen bonds are highlightes as yellow dashed lines.

Table S4. Selected bond lengths, angles and hydrogen bond parameters in the crystal structure of $(NH_4)[VO_2(L^1)]$ (**1**)

Atoms	Bond length/Å	Atoms	Bond length/Å	Atoms	Bond length/Å
C1–C2	1.414(2)	N1–N2	1.4086(19)	V1–O1	1.9045(13)
C1–C6	1.401(2)	N2–C8	1.301(2)	V1–O2	1.9792(14)
C1–C7	1.435(2)	O1–C2	1.309(2)	V1–O3	1.6195(16)
C2–C3	1.415(2)	O2–C8	1.301(2)	V1–O4	1.6313(13)
N1–C7	1.291(2)	V1–N1	2.1575(15)		

Atoms	Bond angle/°	Atoms	Bond angle/°	Atoms	Bond angle/°
C2–C1–C6	119.70(14)	O2–C8–N2	122.78(15)	O1–V1–O3	97.27(7)
C2–C1–C7	121.63(14)	N2–N1–C7	114.73(14)	O1–V1–O4	105.29(6)
C6–C1–C7	118.62(14)	V1–N1–C7	129.55(11)	O2–V1–N1	73.16(5)
C1–C2–C3	119.07(16)	V1–N1–N2	115.55(10)	O2–V1–O3	90.93(7)
O1–C2–C1	122.39(14)	N1–N2–C8	108.72(14)	O2–V1–O4	98.73(6)
O1–C2–C3	118.53(16)	V1–O1–C2	137.73(12)	O3–V1–N1	137.50(7)
C2–C3–C4	120.84(18)	V1–O2–C8	119.27(11)	O3–V1–O4	109.25(8)
C1–C6–C5	119.07(16)	O1–V1–N1	81.72(5)	O4–V1–N1	111.96(7)
N1–C7–C1	123.69(15)	O1–V1–O2	150.30(6)		

D–H···A	D-H	H···A	D···A	∠D–H···A	Symmetry code
N4–H4A···O4	0.86(3)	2.04(3)	2.894(2)	175(2)	*x*, *y*, *z*
N4–H4B···N2	0.91(4)	2.04(4)	2.942(3)	172(3)	1–*x*, 1–*y*, 1–*z*
N4–H4C···O5	0.85(3)	2.55(3)	3.085(3)	122(3)	–1+*x*, *y*, 1+*z*
N4–H4D···O2	0.86(4)	2.33(4)	3.128(3)	155(3)	–*x*, 1–*y*, 1–*z*
C3–H3···O6	0.93	2.56	3.220(3)	129	–1+*x*, *y*, *z*
C7–H7···O3	0.93	2.45	3.172(2)	134	1+*x*, *y*, *z*

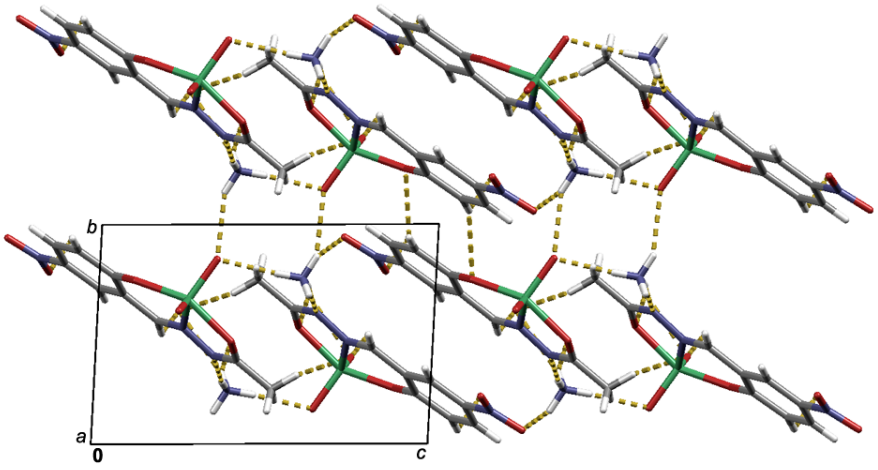

(a)

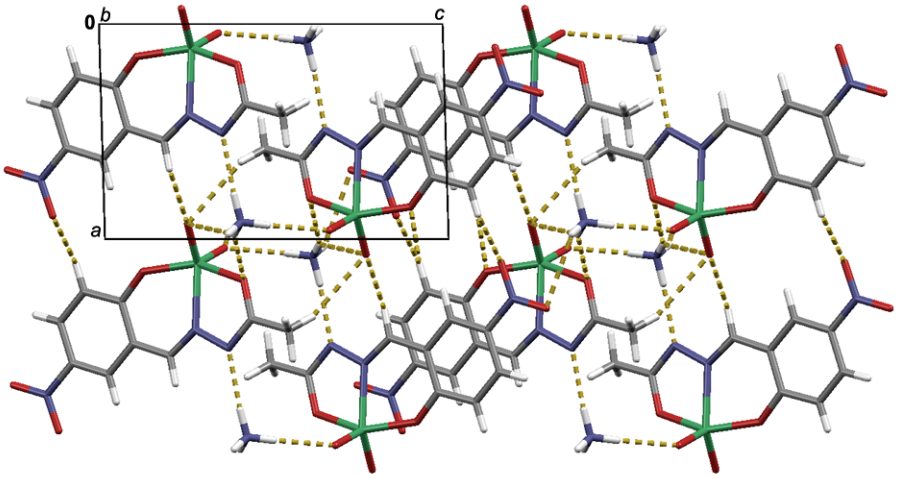

(b)

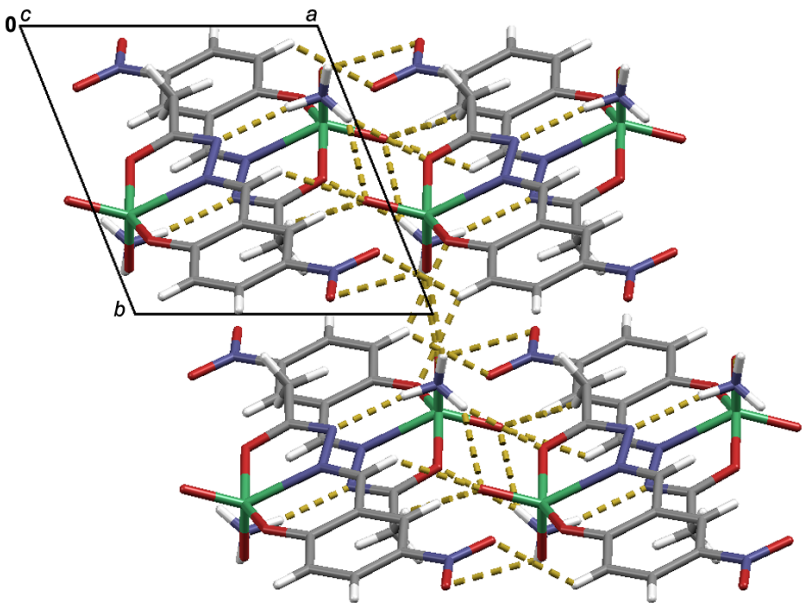

(c)

Figure S17. Crystal packing in $(NH_4)[VO_2(L^1)]$ (**1**) viewed down the: (a) *a*-axis; (b) *b*-axis, and (c) *c*-axis. Hydrogen bonds are highlightes as yellow dashed lines.

Table S5. Selected bond lengths, angles and hydrogen bond parameters in the crystal structure of [VO(L^1)(OMe)(MeOH)] (**2**)

Atoms	Bond length/Å	Atoms	Bond length/Å	Atoms	Bond length/Å
C12–C22	1.420(6)	O11–C21	1.323(5)	V11–O21	1.948(3)
C12–C62	1.394(5)	O12–C22	1.316(5)	V11–O31	1.584(3)
C12–C72	1.436(5)	O21–C81	1.303(6)	V11–O41	2.244(4)
C22–C32	1.397(6)	O22–C82	1.309(5)	V11–O71	1.783(3)
C81–C91	1.497(8)	O41–C111	1.413(7)	V12–N12	2.146(3)
C82–C92	1.472(7)	O41–H41	0.82(4)	V12–O12	1.872(3)
N11–C71	1.292(5)	O42–C112	1.403(7)	V12–O22	1.948(3)
N11–N21	1.408(5)	O42–H42	0.81(4)	V12–O32	1.582(3)
N12–C72	1.283(5)	O71–C101	1.419(6)	V12–O42	2.256(3)
N12–N22	1.400(5)	O72–C102	1.434(7)	V12–O72	1.774(3)
N21–C81	1.299(6)	V11–N11	2.134(3)		
N22–C82	1.302(5)	V11–O11	1.880(3)		

Atoms	Bond angle/°	Atoms	Bond angle/°	Atoms	Bond angle/°
C21–C11–C61	119.0(3)	V11–N11–C71	128.5(3)	O21–V11–O31	98.14(16)
C21–C11–C71	122.6(3)	V11–N11–N21	114.5(2)	O21–V11–O41	79.43(13)
C61–C11–C71	118.4(3)	N22–N12–C72	116.9(4)	O21–V11–O71	97.16(14)
C22–C12–C62	118.7(3)	V12–N12–C72	127.9(3)	O31–V11–N11	92.38(16)
C22–C12–C72	122.3(3)	V12–N12–N22	114.9(2)	O31–V11–O41	175.54(16)
C62–C12–C72	119.1(3)	N11–N21–C81	109.3(3)	O31–V11–O71	100.20(16)
C11–C21–C31	119.7(4)	N12–N22–C82	108.7(3)	O41–V11–N11	83.38(14)
O11–C21–C11	122.7(4)	V11–O11–C21	133.9(3)	O41–V11–O71	83.87(14)
O11–C21–C31	117.6(4)	V12–O12–C22	134.7(3)	O71–V11–N11	165.93(15)
C12–C22–C32	119.6(4)	V11–O21–C81	118.5(3)	O12–V12–N12	83.53(14)
O12–C22–C12	122.0(4)	V12–O22–C82	118.3(3)	O12–V12–O22	152.10(14)
O12–C22–C32	118.4(4)	C111–O41–H41	110(4)	O12–V12–O32	99.73(16)
C21–C31–C41	121.1(4)	V11–O41–C111	125.6(3)	O12–V12–O42	81.45(13)
C22–C32–C42	120.6(4)	V11–O41–H41	125(4)	O12–V12–O72	100.95(15)
C11–C61–C51	119.5(4)	C112–O42–H42	107(5)	O22–V12–N12	74.43(13)
C12–C62–C52	120.7(4)	V12–O42–C112	125.4(3)	O22–V12–O32	98.15(16)
N11–C71–C11	122.5(4)	V12–O42–H42	128(4)	O22–V12–O42	79.25(13)
N12–C72–C12	123.4(4)	V11–O71–C101	127.3(3)	O22–V12–O72	96.67(15)
N21–C81–C91	119.5(4)	V12–O72–C102	128.3(3)	O32–V12–N12	92.52(16)
O21–C81–C91	117.7(4)	O11–V11–N11	83.92(14)	O32–V12–O42	175.63(16)
O21–C81–N21	122.8(4)	O11–V11–O21	152.68(14)	O32–V12–O72	100.38(16)
N22–C82–C92	120.3(4)	O11–V11–O31	99.53(16)	O42–V12–N12	83.42(13)
O22–C82–C92	116.5(4)	O11–V11–O41	81.46(13)	O42–V12–O72	83.47(14)
O22–C82–N22	123.3(4)	O11–V11–O71	100.02(15)	O72–V12–N12	165.34(15)
N21–N11–C71	116.8(3)	O21–V11–N11	74.66(13)		

D–H···A	D-H	H···A	D···A	∠D–H···A	Symmetry code
O41–H41···N22	0.82(4)	1.95(4)	2.770(5)	175(5)	*x*, *y*, *z*
O42–H42···N21	0.81(4)	1.98(5)	2.776(5)	168(7)	1+*x*, *y*, *z*
C102–H10F···O31	0.96	2.58	3.474(7)	155	1+*x*, –1+*y*, *z*
C41–H41A···O62	0.93	2.46	3.126(7)	129	–*x*, 1–*y*, 1–*z*
C42–H42A···O61	0.93	2.46	3.126(7)	128	–*x*, –*y*, 1–*z*
C71–H71···O52	0.93	2.58	3.435(6)	153	–*x*, –*y*, 1–*z*
C72–H72···O51	0.93	2.57	3.426(6)	154	–*x*, 1–*y*, 1–*z*

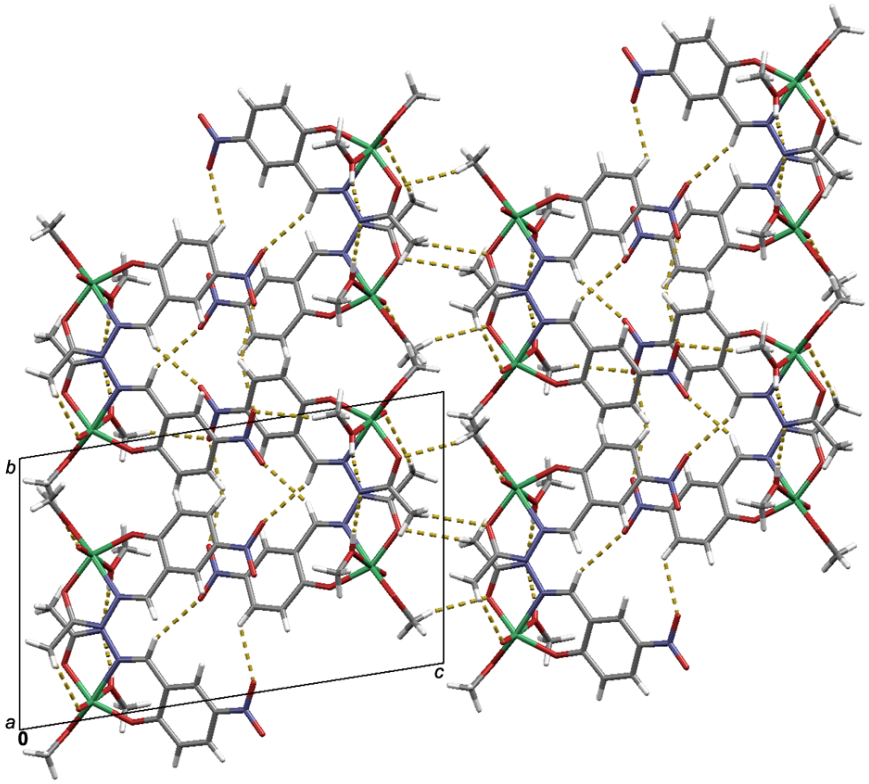

(a)

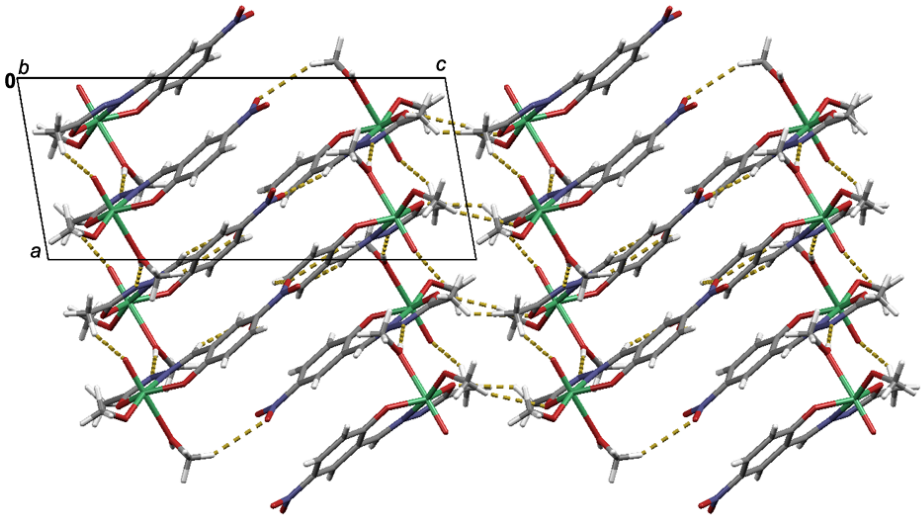

(b)

Figure S18. Crystal packing in [VO(L[1])(OMe)(MeOH)] (**2**) viewed down the: (a) *a*-axis; (b) *b*-axis. Hydrogen bonds are highlightes as yellow dashed lines.

Table S6. Selected bond lengths, angles and hydrogen bond parameters in the crystal structure of $[VO_2(HL^3)]_2 \cdot 2H_2O$ (**5**)

Atoms	Bond length/Å	Atoms	Bond length/Å	Atoms	Bond length/Å
C2–C3	1.418(2)	O3–C9	1.2514(19)	V1–O4	1.6578(10)
N1–C8	1.2878(19)	V1–N1	2.1807(12)	V1–O5	1.6199(12)
N1–N2	1.3835(19)	V1–O1	1.8872(12)		
N2–H2	0.840(16)	V1–O3	2.0432(10)		
O1–C2	1.3237(17)	V1–O4_a	2.3420(11)		

Atoms	Bond angle/°	Atoms	Bond angle/°	Atoms	Bond angle/°
C2–C1–C6	119.84(13)	N2–N1–C8	117.89(12)	O1–V1–O4_a	84.73(4)
C2–C1–C8	121.82(13)	V1–N1–C8	129.40(11)	O1–V1–O5	100.98(6)
C6–C1–C8	118.31(14)	V1–N1–N2	112.67(9)	O3–V1–N1	73.27(5)
C1–C2–C3	118.42(13)	C9–N2–H2	122.7(13)	O3–V1–O4	94.09(5)
O1–C2–C1	123.59(12)	N1–N2–C9	113.96(13)	O3–V1–O4_a	76.73(4)
O1–C2–C3	117.91(13)	N1–N2–H2	123.1(14)	O3–V1–O5	95.49(6)
C2–C3–C4	120.33(15)	V1–O1–C2	132.34(10)	O4–V1–N1	153.91(6)
O2–C3–C2	114.50(13)	V1–O3–C9	119.77(10)	O4–V1–O4_a	78.60(5)
C1–C6–C5	120.35(16)	V1–O4–V1_a	101.40(5)	O4–V1–O5	106.34(6)
N1–C8–C1	121.94(13)	N1–V1–O4_a	76.33(4)	O5–V1–N1	97.68(6)
N2–C9–C10	119.04(15)	O1–V1–N1	82.34(5)	O5–V1–O4_a	171.22(6)
O3–C9–C10	120.93(15)	O1–V1–O3	152.15(5)		
O3–C9–N2	120.03(14)	O1–V1–O4	102.49(5)		

D–H···A	D-H	H···A	D···A	∠D–H···A	Symmetry code
N2–H2···O6	0.840(16)	1.847(16)	2.6849(19)	175(2)	*x*, *y*, *z*
O6–H6A···O3	0.79(3)	2.31(3)	2.9259(17)	135(3)	1+*x*, *y*, *z*
O6–H6B···O5	0.81(2)	1.99(2)	2.7913(18)	169(3)	1–*x*, 1–*y*, 2–*z*
C8–H8···O4	0.93	2.31	3.0514(17)	137	1+*x*, *y*, *z*

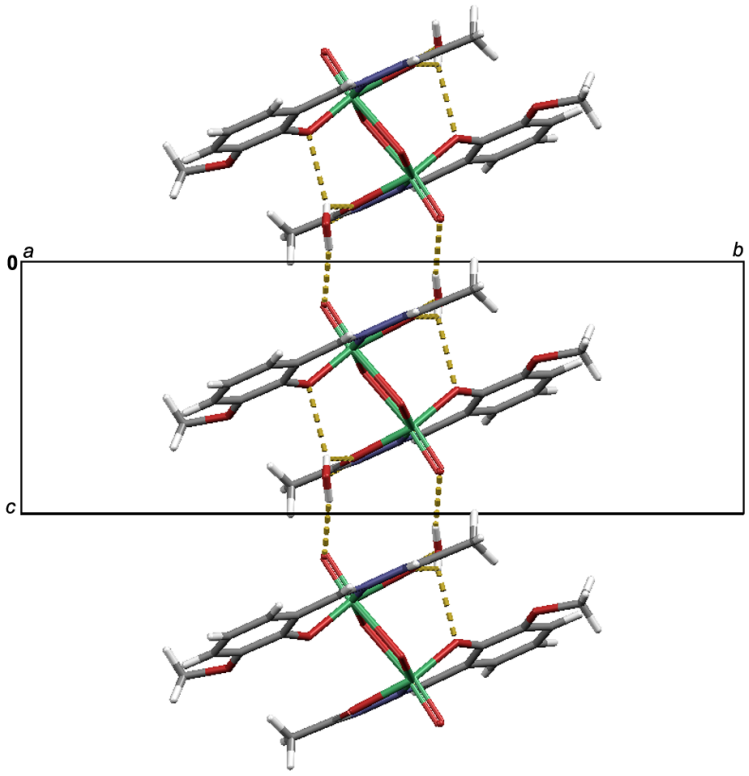

(a)

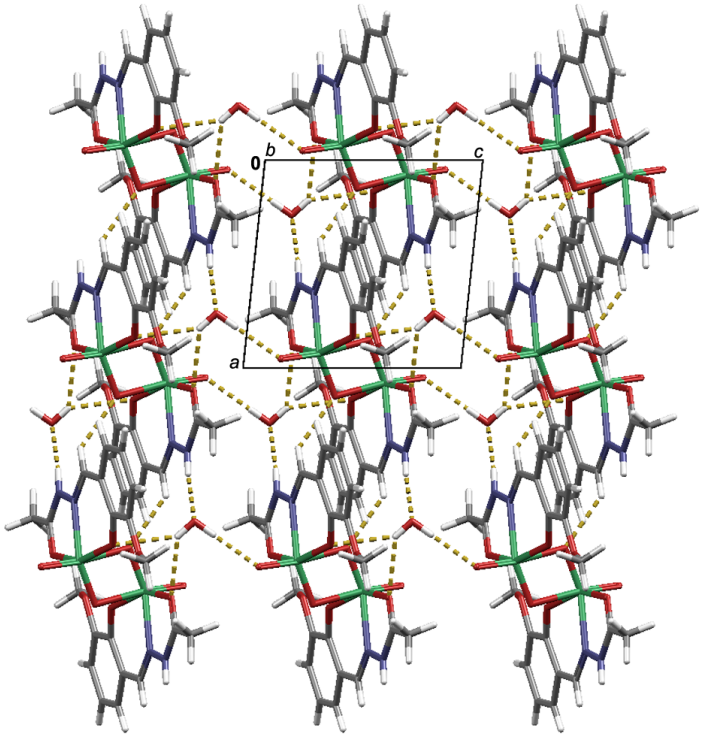

(b)

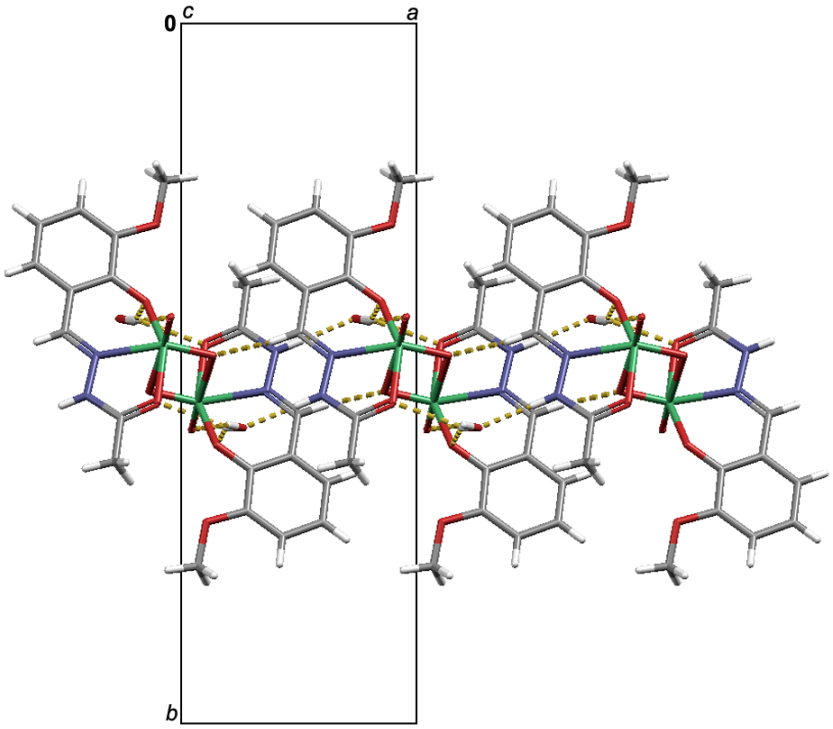

(c)

Figure S19. Supramolecular layers formed in formed in *ac*-plane in $[VO_2(HL^3)]_2 \cdot 2H_2O$ (**6**) viewed down the: (a) *a*-axis; (b) *b*-axis, (c) *c*-axis. Hydrogen bonds are highlighted as yellow dashed lines. Hydrogen bonds are highlightes as yellow dashed lines.

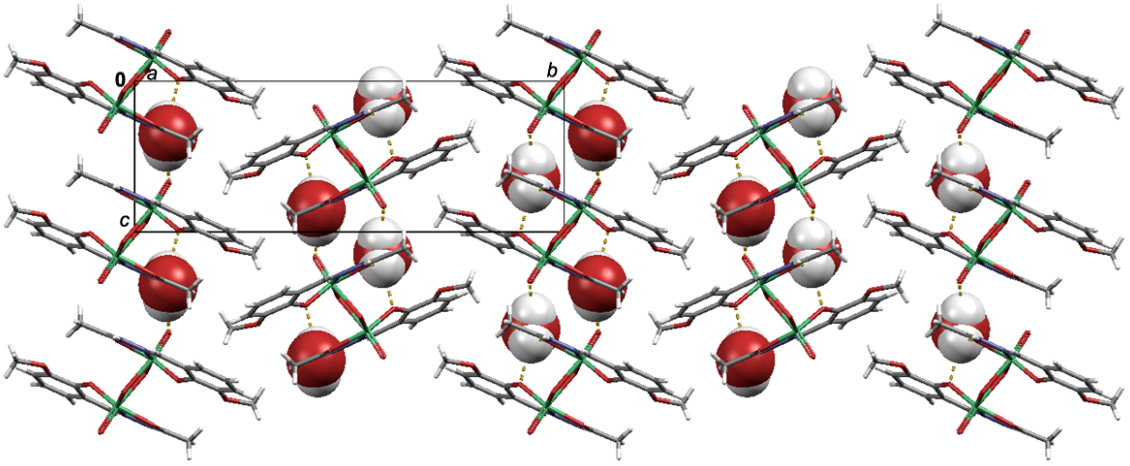

(a)

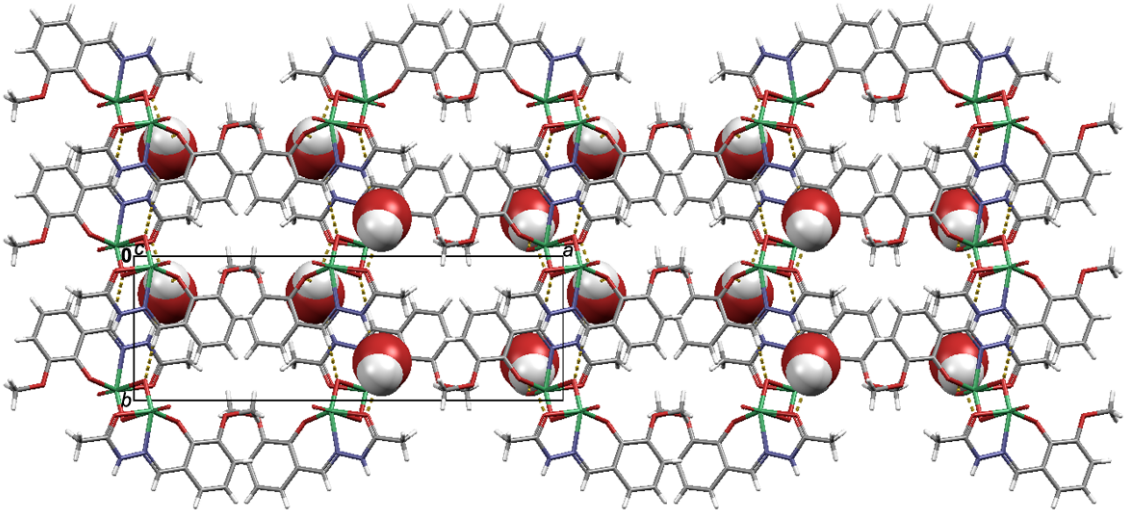

(b)

Figure S20. Crystal packing in $[VO_2(HL^3)]_2 \cdot 2H_2O$ (**6**) viewed down the: (a) *a*-axis; (b) *c*-axis. Crystal water molecules are highlighted in spacefill style. Hydrogen bonds are highlightes as yellow dashed lines.

Table S7. Selected bond lengths, angles and hydrogen bond parameters in the crystal structure of [VO(L^3)(OMe)(MeOH)] (**7**)

Atoms	Bond length/Å	Atoms	Bond length/Å	Atoms	Bond length/Å
C1–C2	1.405(2)	N2–C9	1.306(2)	V1–N1	2.1133(12)
C1–C6	1.411(2)	O1–C2	1.3285(19)	V1–O1	1.8530(12)
C1–C8	1.436(2)	O3–C9	1.2917(19)	V1–O3	1.9708(12)
C2–C3	1.413(2)	O5–C12	1.389(3)	V1-O6	1.5868(14)
C9–C10	1.492(2)	O4–C11	1.404(2)		
N1–C8	1.286(2)	V1–O4	1.7661(12)		
N1–N2	1.3958(17)	V1–O5	2.3279(13)		

Atoms	Bond angle/°	Atoms	Bond angle/°	Atoms	Bond angle/°
C2–C1–C6	119.71(15)	V1–O5–C12	128.06(13)	O1–V1–O4	104.84(5)
C2–C1–C8	121.40(14)	V1–O4–C11	130.91(13)	O1–V1–O5	79.96(5)
C6–C1–C8	118.78(15)	V1–N1–C8	126.39(10)	O1–V1–O6	100.39(6)
C1–C2–C3	119.02(13)	V1–N1–N2	115.94(9)	O3–V1–N1	74.26(5)
O1–C2–C1	122.29(14)	N1–N2–C9	108.77(12)	O3–V1–O4	91.08(5)
O1–C2–C3	118.57(14)	V1–O1–C2	132.43(10)	O3–V1–O5	81.21(5)
C2–C3–C4	119.73(15)	V1–O3–C9	118.13(10)	O3–V1–O6	96.42(6)
O2–C3–C2	114.98(13)	O1–V1–N1	84.17(5)	O4–V1–N1	158.80(5)
C1–C6–C5	120.20(17)	O1–V1–O3	153.47(5)		
N1–C8–C1	124.14(14)	O4–V1–O6	102.96(6)		
N2–C9–C10	119.37(14)	O5–V1–N1	80.01(5)		
O3–C9–C10	117.76(14)	O5–V1–O6	173.94(6)		
O3–C9–N2	122.87(14)	O6–V1–N1	93.99(6)		
N2–N1–C8	117.27(13)	O4–V1–O5	82.71(5)		

D–H···A	D-H	H···A	D···A	∠D–H···A	Symmetry code
O5–H5···N2	0.73(2)	2.04(2)	2.7675(19)	176(2)	1-*x*,1-*y*,1-*z*
C7–H7B···O6	0.96	2.56	3.450(3)	153	*x*,3/2-*y*,1/2+*z*
C4–H4···O6	0.93	2.48	3.376(2)	161	-*x*,-1/2+*y*,3/2-*z*
C5–H5A···O2	0.93	2.54	3.382(2)	151	-*x*,-1/2+*y*,3/2-*z*

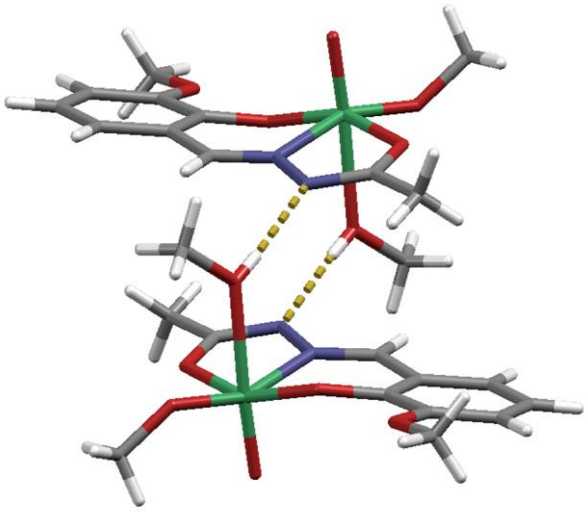

(a)

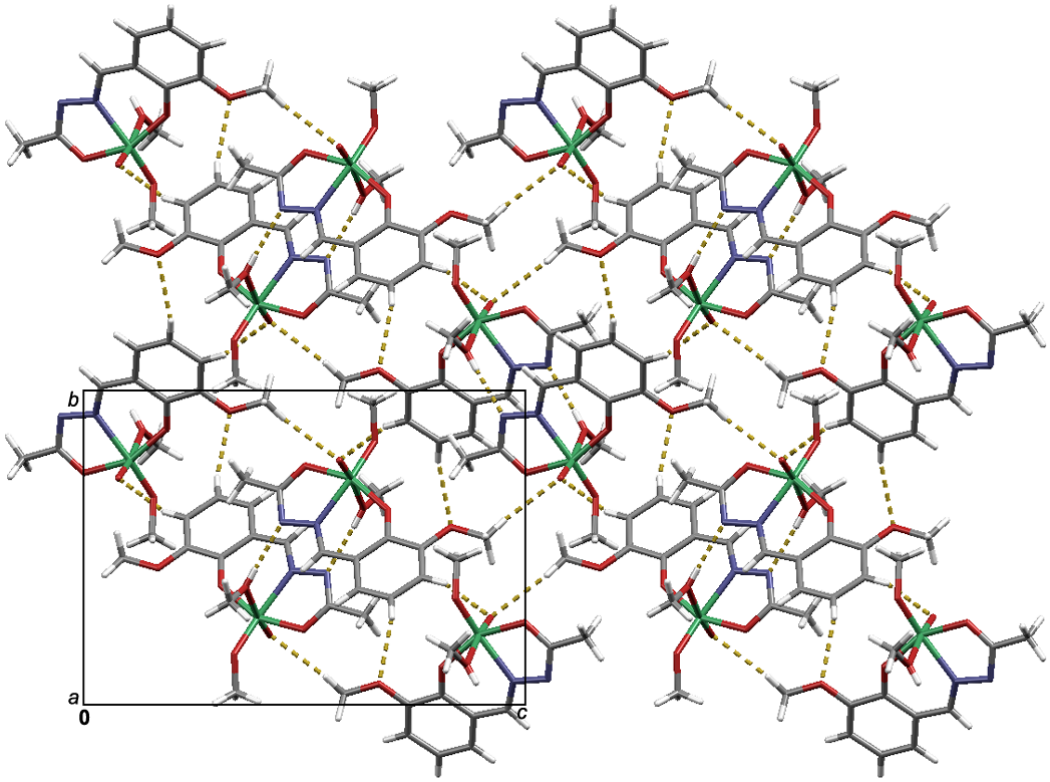

(b)

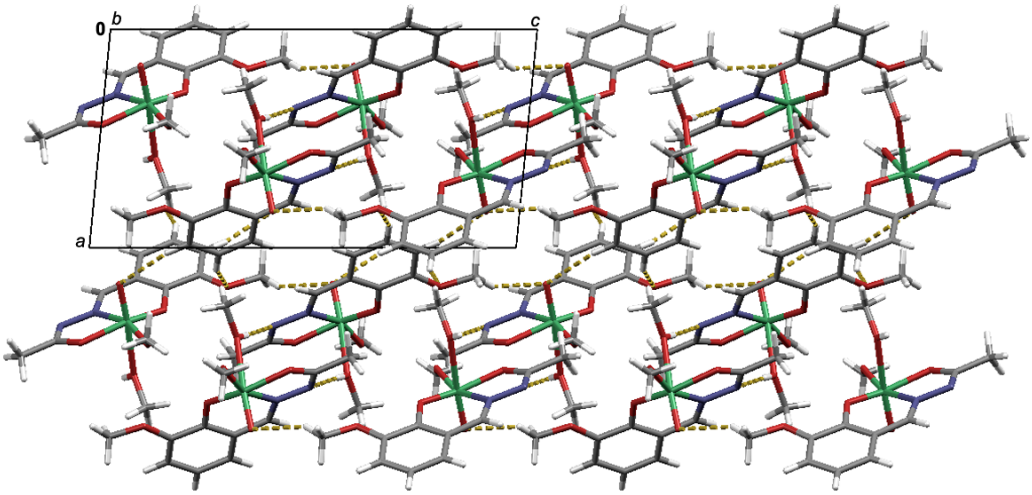

(c)

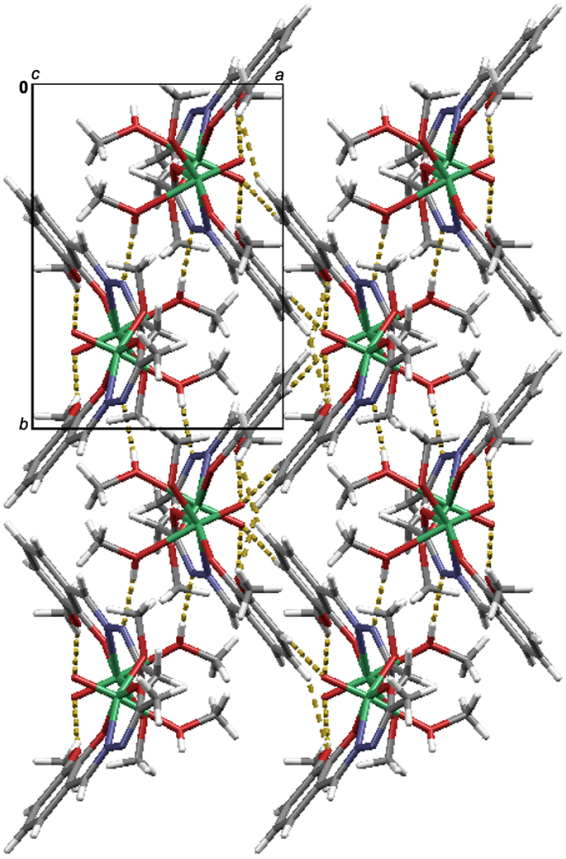

(d)

Figure S21. (a) Supramolecular dimers formed through $R_2^2(10)$ hydrogen bonded motif. Crystal packing in [VO(L^3)(OMe)(MeOH)] (**7**) viewed down the: (b) *a*-axis; (c) *b*-axis, and (d) *c*-axis. Non-coordinated methanol molecules are presented in the spacefill style. Hydrogen bonds are highlightes as yellow dashed lines.

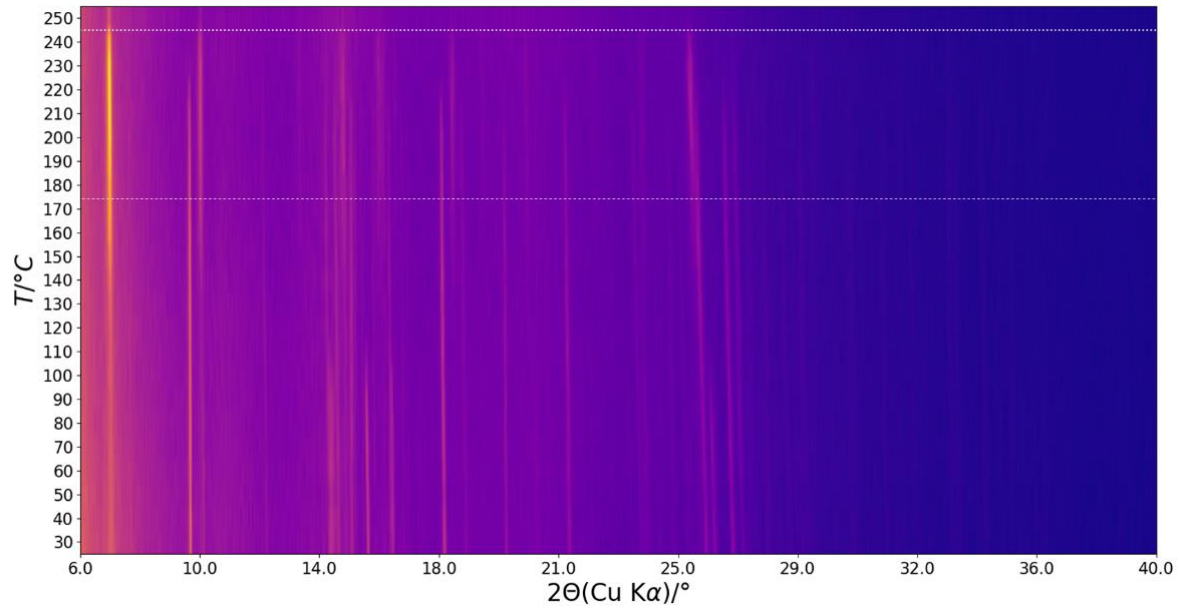

Figure S22. Temperature-dependent diffraction patterns of $(NH_4)[VO_2(L^1)]$ (**1**)

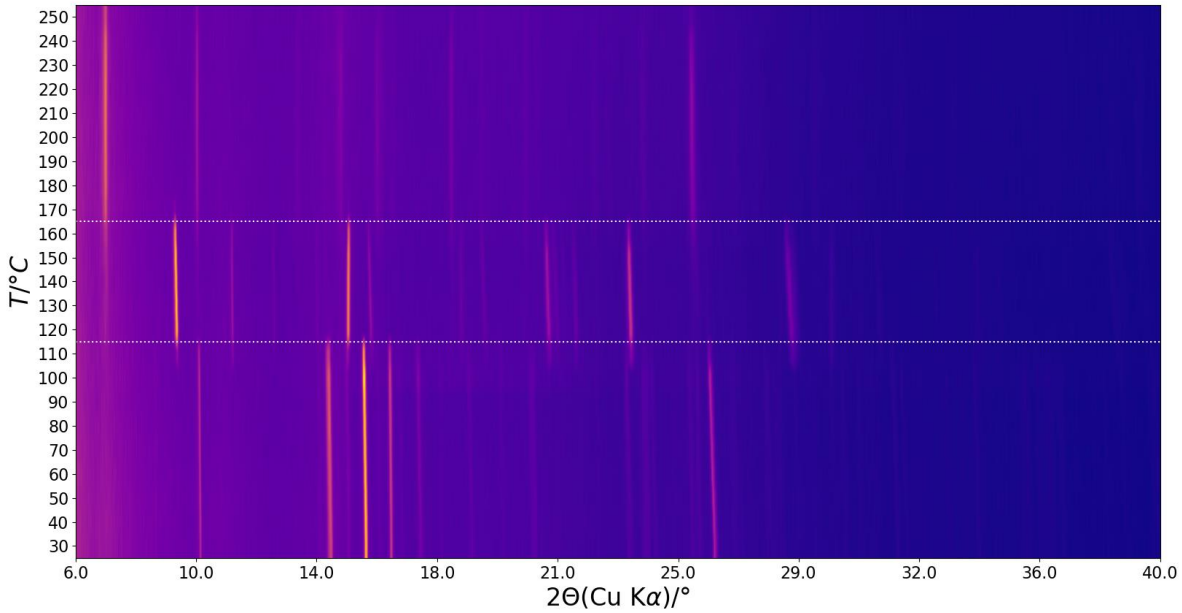

Figure S23. Temperature-dependent diffraction patterns of $[VO(L^1)(OMe)(MeOH)]$ (**2**)

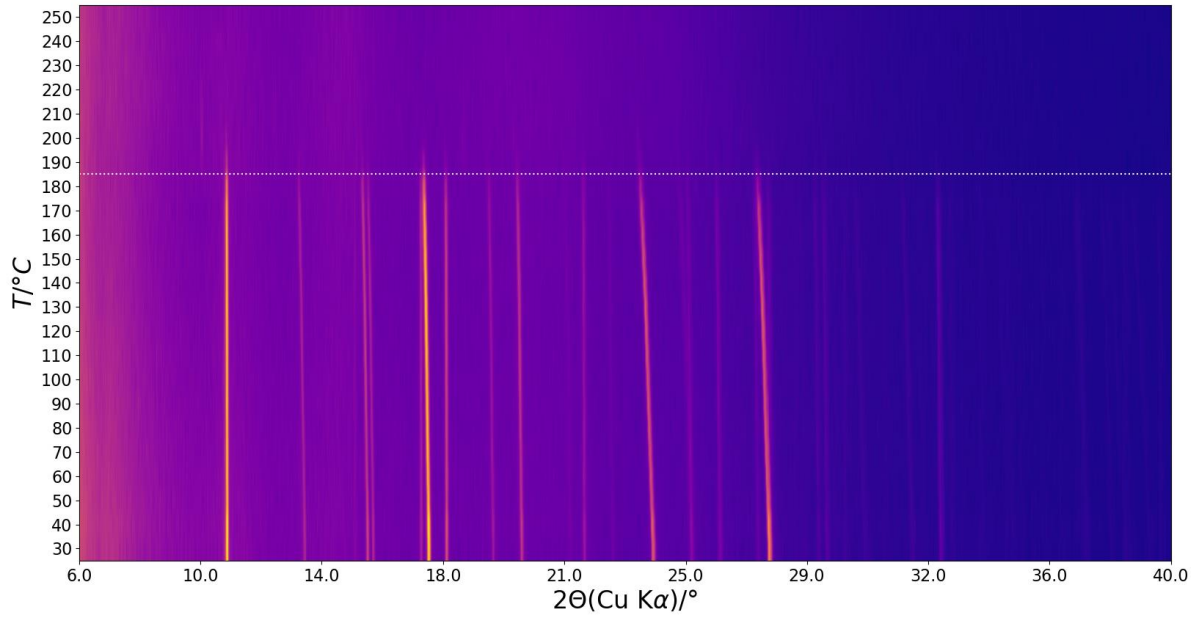

Figure S24. Temperature-dependent diffraction patterns of $[VO_2(HL^2)]$ (**4**)

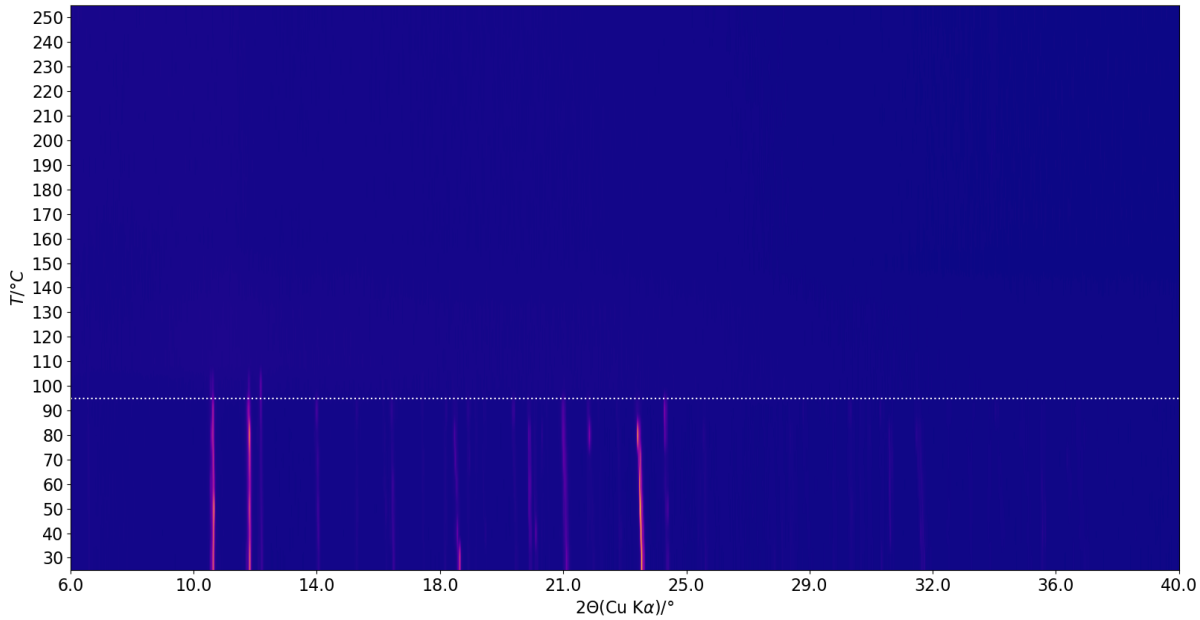

Figure S25. Temperature-dependent diffraction patterns of $[VO(L^3)(OEt)(H_2O)]$ (**5**)

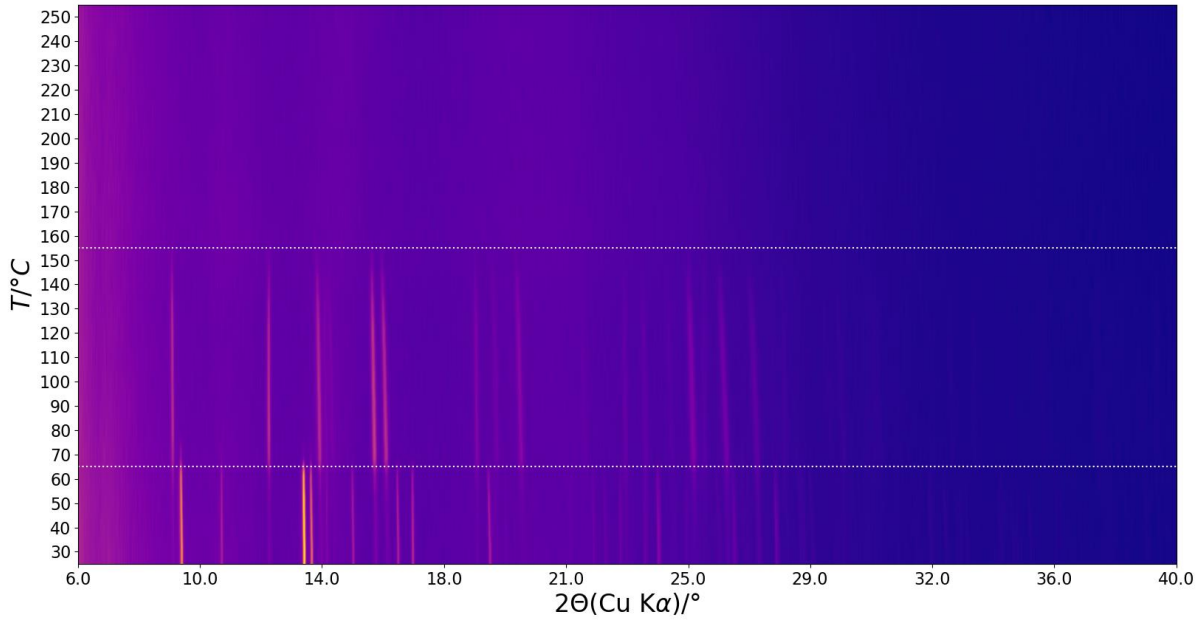

Figure S26. Temperature-dependent diffraction patterns of [VO(L^3)(OMe)(MeOH)] (**7**)

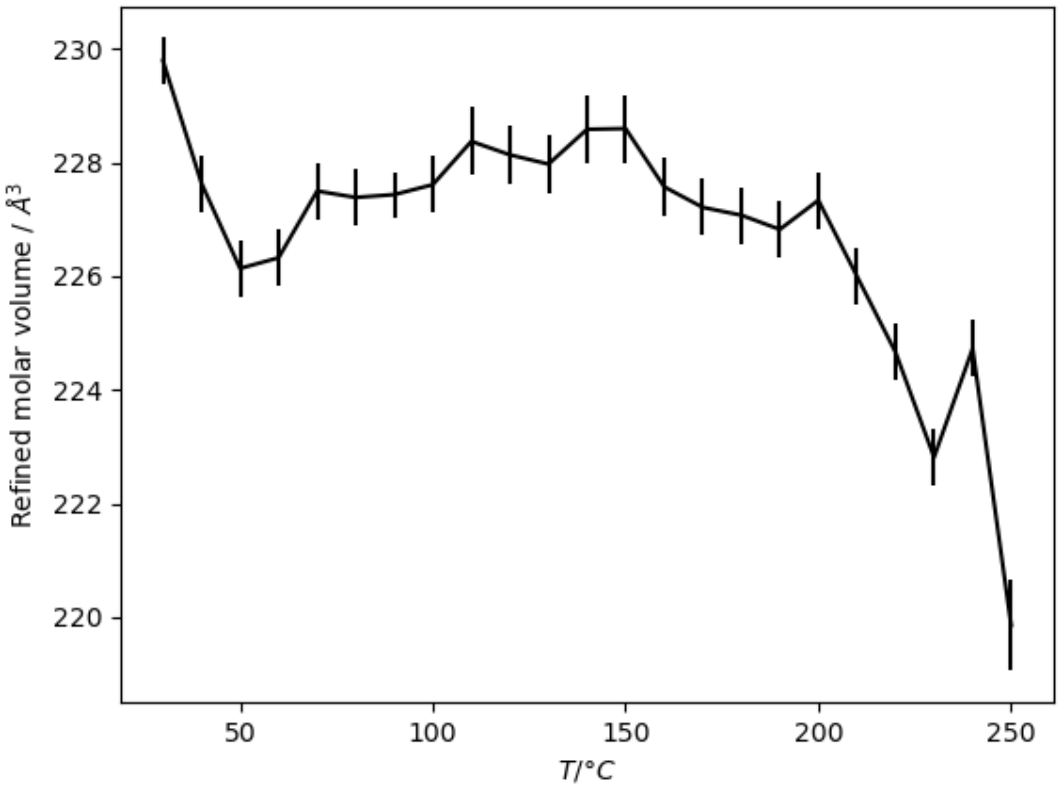

Figure S27. Temperature dependence of refined molar volume of the (NH_4)[VO_2(L^1)] (**1**) compound, which is calculated as $\frac{1}{8}V_{cell}$. Vertical bars represent standard uncertainty. Due to poor crystallinity of the compound, and consequently low diffraction data quality, the molar volume could not be refined precisely, but the overall change across the whole temperature range is insignificant - around 2%. However, above 160 °C the sample converts to another phase with similar unit cell parameters.

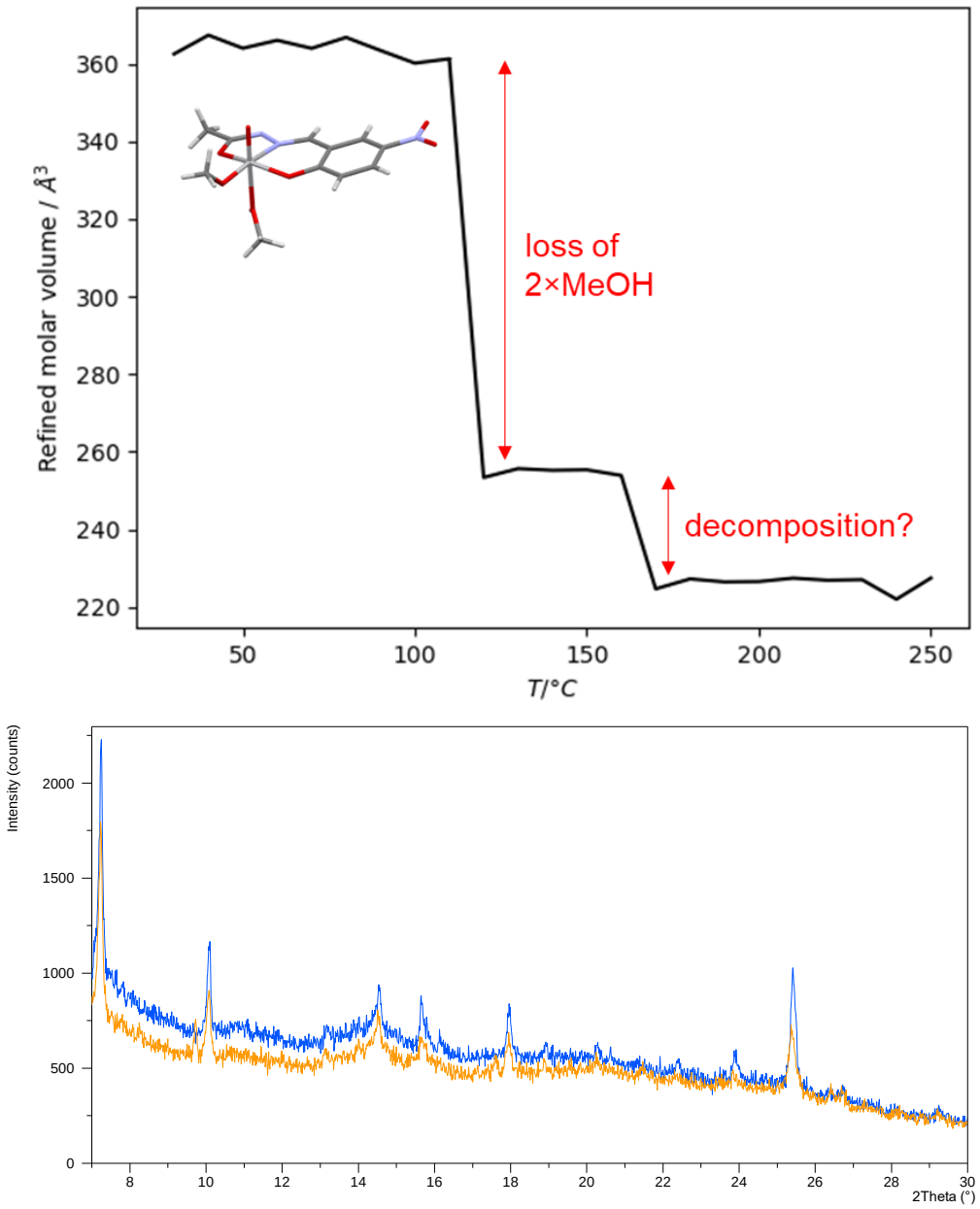

Figure S28. (Top) Temperature dependence of refined molar volume of the [VO(L^1)(OMe)(MeOH)] (**2**) compound, which is calculated as $\frac{1}{4}V_{cell}$ below 160 °C, and $\frac{1}{8}V_{cell}$ above it. Standard uncertainties are very low, and not visible in the graph. At low temperatures the molar volume corresponds to the VO(L) moiety ligated with methoxy/methanol ligands. Above 110 °C the change in molar volume corresponds to the loss of two methanol molecules per moiety (ca. 100 Å^3 as calculated from methanol crystal structure). (Bottom) Above 160 °C sample probably converts to [VO_2(HL^1)], the same phase observed in high temperature PXRD patterns of (NH_4)[VO_2(L^1)] (**1**).

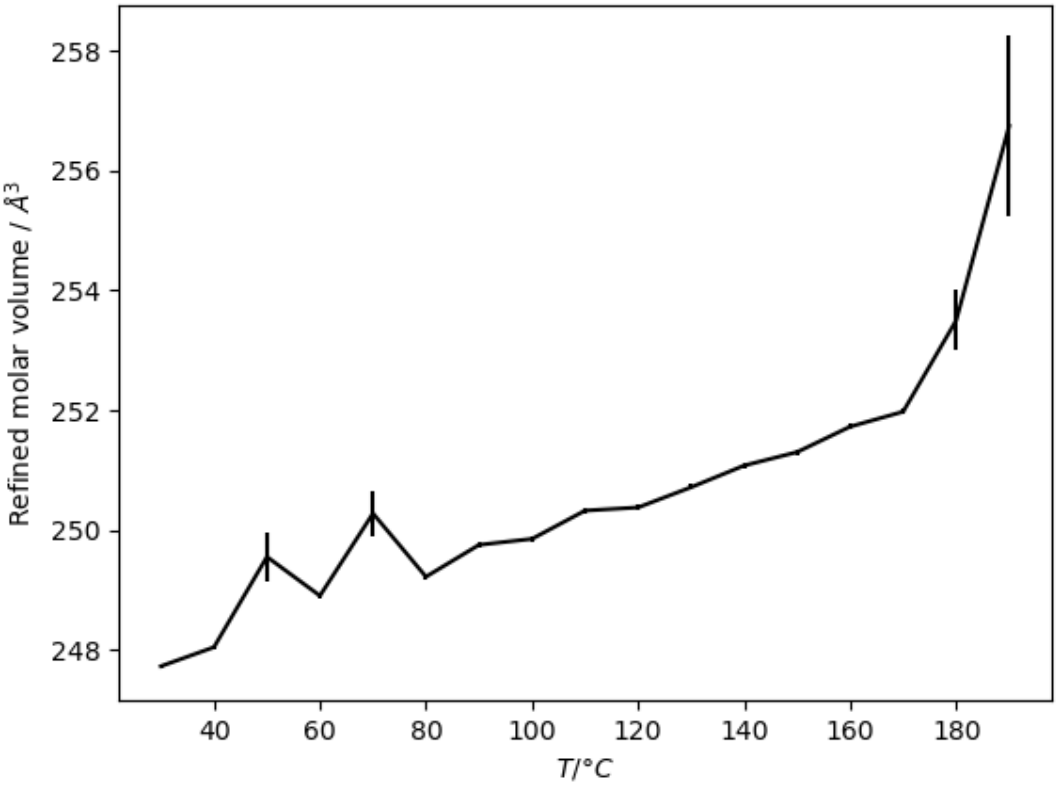

Figure S29. Temperature dependence of refined molar volume of the $[VO_2(HL^2)]$ (**4**) compound, which is calculated as $\frac{1}{4}V_{cell}$. Vertical bars represent standard uncertainty. Molar volume increases smoothly across the whole temperature range, and the overall change across the whole temperature range is insignificant - around 4%. Partial amorphization begins at around 180 °C, as evidenced by high uncertainty of molar volume at those temperatures.

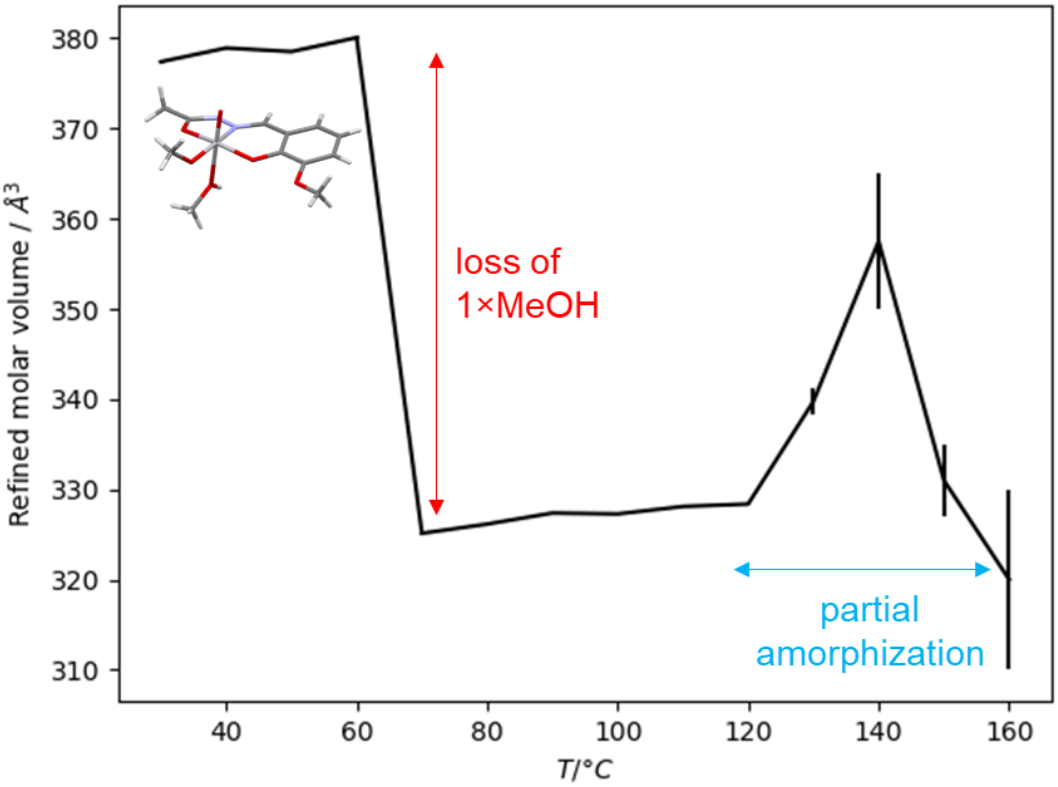

Figure S30. Temperature dependence of refined molar volume of the [VO(L[3])(OMe)(MeOH)] (**7**) compound, which is calculated as $\frac{1}{4}V_{cell}$. Vertical bars represent standard uncertainty. At low temperatures the molar volume corresponds to the VO(L) moiety ligated with methoxy/methanol ligands. Above 60 °C the change in molar volume corresponds to loss of one methanol molecule per moiety (ca. 50 Å^3 as calculated from methanol crystal structure). Above 120 °C partial amorphization of the sample prevents precise refinements of molar volume.

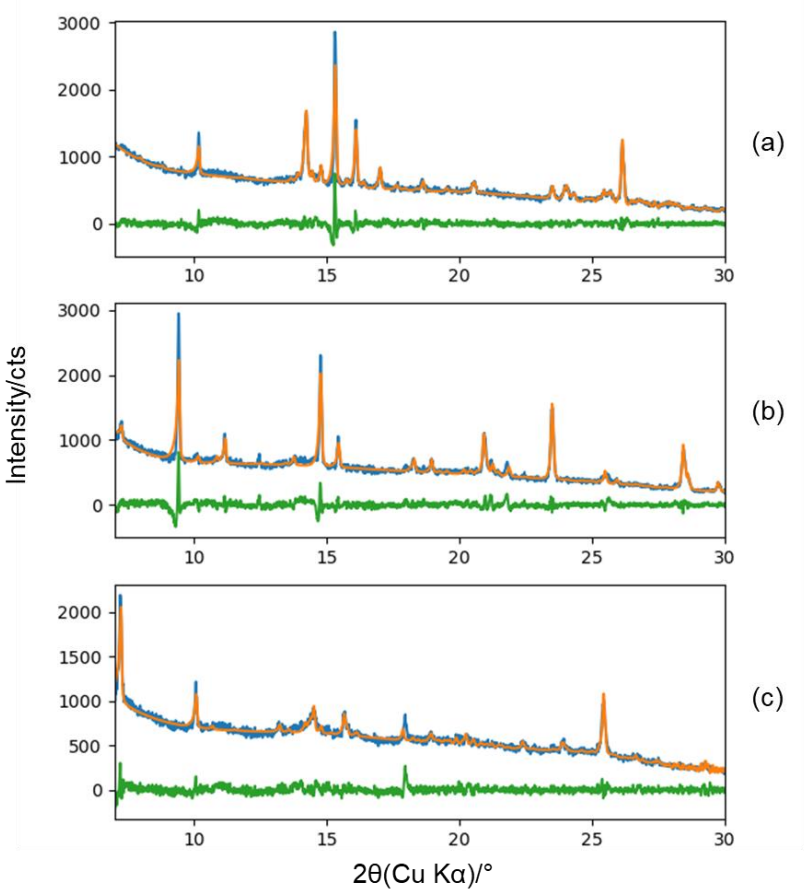

Figure S31. Examples of le Bail refinement on temperature-dependent PXRD data of [VO(L^1)(OMe)(MeOH)] (**2**), at (a) 30 °C using unit cell parameters of [VO(L^1)(OMe)(MeOH)], (b) 140 °C, unit cell parameters of intermediate phase: a = 13.310(3) Å, b = 9.9181(17) Å, c = 8.6416(14) Å, α = 100.751(18)°, β = 108.367(10)°, γ = 101.710(17)°, (c) 200 °C, unit cell parameters of [VO_2(HL^1)], a = 15.2143(15) Å, b = 12.8189(13) Å, c = 9.7818(11) Å, α = 107.074(10)°, β = 93.985(11)°, γ = 93.584(9)°. The refinement results for (c) are similar to high temperature phase of (NH_4)[VO_2(L^1)] results.

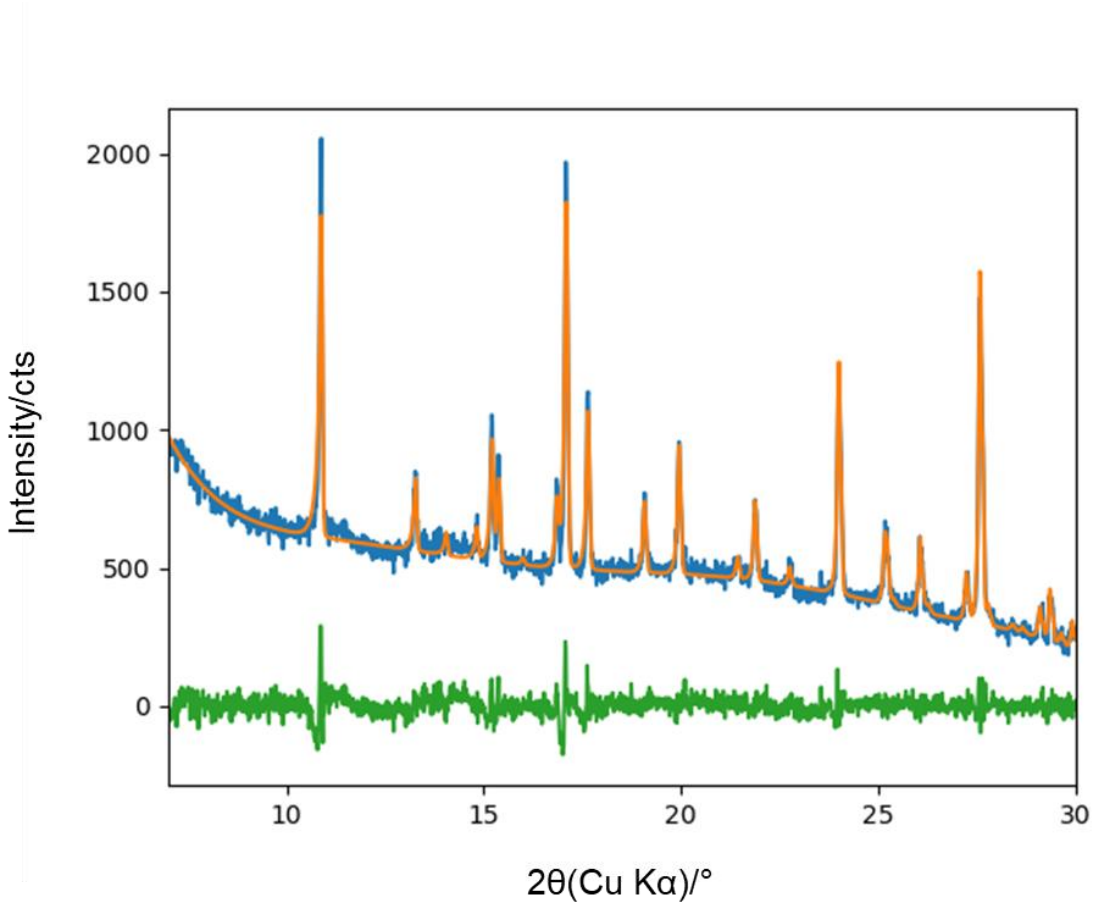

Figure S32. Example of le Bail refinement on temperature-dependent PXRD data of $[VO_2(HL^2)]$ (**4**), at 30 °C using unit cell parameters of $[VO_2(HL^2)]$ (**4**).

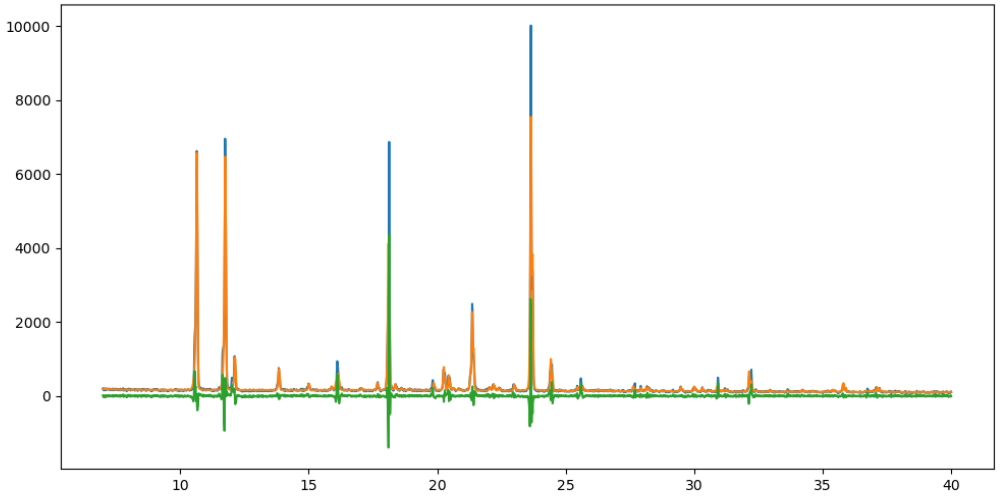

Figure S33. Example of le Bail refinement on temperature-dependent PXRD dana of $[VO(L^3)(OEt)(H_2O)]$ (**5**), at 30 °C using cell parameters of $[VO(L^3)(OEt)(H_2O)]$ (**5**).

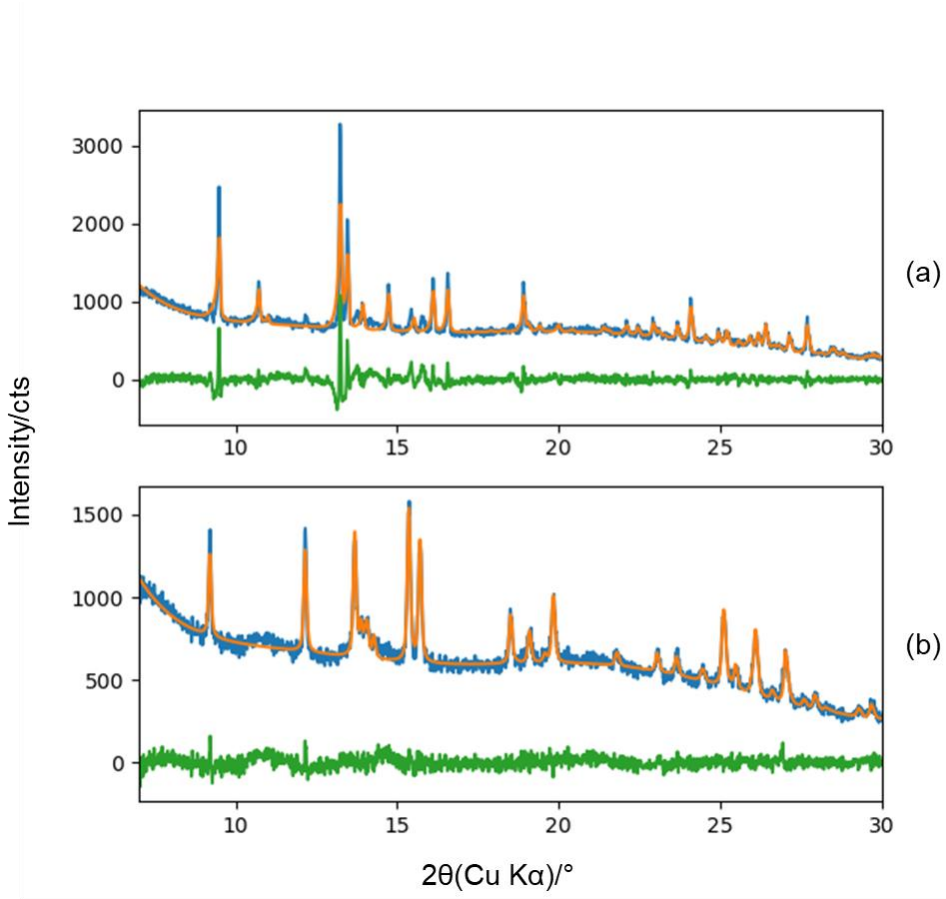

Figure S34. Examples of le Bail refinement on temperature-dependent PXRD data of [VO(L^3)(OMe)(MeOH)] (**7**), at (a) 30 °C using unit cell parameters of [VO(L^3)(OMe)(MeOH)] (**7**), (b) 100 °C, unit cell parameters of high-temperature phase: a = 14.532(3) Å, b = 12.726(3) Å, c = 7.0829(10) Å, $\alpha = \gamma = 90$ °, $\beta = 92.019(9)$°.

Table S8. Tabulated weighted residual (R_{wp}) and unit cell parameters refined by le Bail fit from temperature-dependent PXRD data.

Sample	*T* / °C	R_{wp}	*a*/Å	*b*/Å	*c*/Å	*α*/°	*β*/°	*γ*/°	*V*/Å³
$(NH_4)[VO_2(L^1)]$ (**1**)	30	5.604	15.250(6)	12.994(7)	9.819(5)	106.52(2)	93.52(3)	94.02(4)	1854.1(16)
	40	5.736	15.251(5)	12.997(6)	9.805(5)	106.46(2)	93.40(3)	94.10(3)	1852.6(15)
	50	5.587	15.265(7)	13.013(7)	9.809(6)	106.40(2)	93.36(4)	94.10(4)	1858.0(17)
	60	5.740	15.303(6)	13.064(8)	9.874(6)	106.49(2)	93.45(4)	93.99(4)	1881.5(18)
	70	5.867	15.309(7)	13.072(8)	9.861(6)	106.40(2)	93.29(3)	94.04(4)	1882.2(18)
	80	5.644	15.327(6)	13.078(7)	9.850(6)	106.32(2)	93.24(3)	94.06(4)	1884.0(17)
	90	5.692	15.330(7)	13.080(7)	9.866(6)	106.33(2)	93.22(3)	94.09(3)	1887.6(18)
	100	5.660	15.349(7)	13.091(8)	9.875(6)	106.28(3)	93.21(4)	94.07(4)	1893.9(19)
	110	5.376	15.327(5)	13.055(6)	9.977(4)	106.15(2)	92.25(3)	94.25(3)	1908.7(13)
	120	5.492	15.334(6)	13.062(7)	10.004(6)	106.06(3)	92.39(5)	94.26(4)	1916.1(18)
	130	5.345	15.352(5)	13.075(5)	10.003(6)	105.97(2)	92.48(5)	94.24(3)	1920.8(15)
	140	5.815	15.376(7)	13.138(7)	9.984(5)	105.74(3)	92.31(5)	94.50(3)	1931.3(16)
	150	5.888	15.405(7)	13.091(8)	10.062(5)	105.73(3)	91.64(5)	94.76(4)	1943.7(18)
	160	5.840	15.396(7)	13.069(6)	10.077(4)	105.67(3)	91.27(4)	94.87(3)	1943.1(15)
	170	5.619	15.391(6)	13.046(9)	10.043(5)	105.87(3)	91.37(3)	94.88(3)	1930.3(18)
	180	5.655	15.398(6)	13.063(7)	10.050(4)	105.86(3)	91.29(3)	94.87(3)	1935.3(15)
	190	5.961	15.408(6)	13.051(7)	10.053(3)	105.86(3)	91.41(3)	94.89(3)	1935.1(14)
	200	5.871	15.406(8)	13.039(10)	10.047(5)	105.87(3)	91.27(4)	94.97(4)	1932(2)
	210	5.567	15.414(9)	13.038(11)	10.045(5)	105.86(3)	91.33(4)	95.01(5)	1932(2)
	220	4.923	15.389(15)	12.789(14)	9.975(7)	105.49(5)	90.49(5)	95.56(8)	1882(3)
	230	5.021	15.426(17)	12.823(14)	9.993(7)	105.49(4)	91.00(7)	94.74(10)	1897(3)
	240	4.931	15.361(17)	12.739(18)	9.972(9)	105.42(6)	90.63(8)	94.70(11)	1874(4)
	250	4.552	15.52(7)	12.68(9)	9.87(6)	105.53(18)	91.2(2)	94.8(4)	1862(19)
$[VO(L_1)(OMe)(MeOH)]$ (**2**)	30	6.582	7.5592(10)	11.0960(18)	17.737(3)	81.464(13)	80.358(10)	89.829(10)	1450.1(4)
	40	6.844	7.5879(11)	11.1493(18)	17.823(3)	81.331(13)	80.444(9)	89.822(10)	1469.5(4)
	50	6.725	7.5709(9)	11.1098(19)	17.766(4)	81.375(15)	80.323(12)	89.830(11)	1456.0(4)
	60	6.890	7.5836(9)	11.1283(18)	17.803(4)	81.425(14)	80.342(11)	89.839(10)	1464.2(4)
	70	6.865	7.5774(10)	11.104(2)	17.758(4)	81.387(15)	80.328(11)	89.819(10)	1455.9(5)
	80	6.701	7.5924(10)	11.1347(19)	17.821(4)	81.304(13)	80.211(13)	89.848(9)	1467.2(4)

	90	7.480	7.5401(11)	11.119(2)	17.791(3)	81.407(15)	80.382(12)	89.890(13)	1453.7(5)
	100	7.600	7.5317(12)	11.077(2)	17.725(4)	81.451(17)	80.208(15)	89.708(15)	1440.6(5)
	110	7.904	7.5292(11)	11.091(3)	17.760(4)	81.640(19)	80.126(14)	89.897(12)	1445.1(5)
	120	8.328	13.280(3)	9.9195(18)	8.6376(15)	100.928(17)	108.759(11)	101.848(17)	1013.5(4)
	130	7.944	13.309(3)	9.9230(16)	8.6575(16)	100.913(18)	108.457(10)	101.534(16)	1022.6(4)
	140	8.060	13.310(3)	9.9181(17)	8.6416(14)	100.751(18)	108.367(10)	101.710(17)	1020.9(4)
	150	8.060	13.313(3)	9.9207(17)	8.6342(13)	100.596(16)	108.265(11)	101.826(16)	1021.4(3)
	160	7.658	13.262(3)	9.924(3)	8.6355(15)	100.696(17)	108.400(13)	101.979(17)	1015.6(4)
	170	5.673	15.1799(17)	12.7879(10)	9.7514(13)	107.196(11)	93.952(11)	93.550(11)	1797.3(4)
	180	6.071	15.2240(14)	12.8235(12)	9.7956(10)	106.965(9)	93.894(10)	93.661(7)	1817.9(3)
	190	6.312	15.2128(16)	12.8183(13)	9.7810(11)	107.088(9)	93.974(10)	93.642(8)	1811.7(3)
	200	6.028	15.2143(15)	12.8189(13)	9.7818(11)	107.074(10)	93.985(11)	93.584(9)	1812.4(3)
	210	6.235	15.2355(14)	12.8297(13)	9.7956(10)	107.029(9)	93.849(10)	93.693(8)	1819.5(3)
	220	6.007	15.2254(15)	12.8232(14)	9.7856(12)	107.044(12)	94.025(13)	93.621(10)	1815.1(4)
	230	6.149	15.2302(15)	12.8319(13)	9.7861(11)	107.137(10)	93.958(11)	93.601(9)	1816.3(3)
	240	5.411	15.1059(16)	12.7420(19)	9.7202(11)	107.256(11)	93.824(11)	93.663(10)	1775.9(4)
	250	5.468	15.2285(15)	12.8262(13)	9.7998(11)	106.961(10)	93.907(11)	93.651(8)	1819.6(3)
$[VO_2(HL^2)]$ (**4**)	30	6.037	7.5012(6)	11.9348(11)	11.2087(15)	90	99.081(6)	90	990.89(18)
	40	5.843	7.5098(5)	11.9342(12)	11.2113(13)	90	99.097(6)	90	992.16(17)
	50	13.196	7.523(6)	11.972(10)	11.222(12)	90	99.02(5)	90	998.2(16)
	60	5.774	7.5266(6)	11.9442(13)	11.2157(17)	90	99.100(6)	90	995.6(2)
	70	12.684	7.538(5)	11.980(10)	11.224(12)	90	99.00(5)	90	1001.1(15)
	80	5.674	7.5396(6)	11.9410(13)	11.2139(15)	90	99.106(6)	90	996.87(19)
	90	6.091	7.5491(6)	11.9462(14)	11.2193(16)	90	99.121(7)	90	999.0(2)
	100	5.699	7.5544(6)	11.9442(14)	11.2181(15)	90	99.130(6)	90	999.40(19)
	110	5.910	7.5637(6)	11.9470(13)	11.2232(15)	90	99.143(6)	90	1001.29(19)
	120	6.050	7.5683(6)	11.9461(15)	11.2200(17)	90	99.134(7)	90	1001.5(2)
	130	5.952	7.5763(5)	11.9443(14)	11.2247(15)	90	99.146(6)	90	1002.85(19)
	140	5.876	7.5852(6)	11.9463(15)	11.2258(15)	90	99.150(6)	90	1004.3(2)
	150	5.815	7.5960(6)	11.9435(14)	11.2234(15)	90	99.183(7)	90	1005.2(2)
	160	5.745	7.6048(6)	11.9455(16)	11.2279(16)	90	99.180(7)	90	1006.9(2)

	170	5.533	7.6138(7)	11.9435(17)	11.2273(19)	90	99.188(7)	90	1007.9(2)
	180	9.883	7.641(10)	11.941(14)	11.257(17)	90	99.21(7)	90	1014(2)
	190	5.909	7.69(3)	12.05(4)	11.23(4)	90	99.4(2)	90	1027(6)
	200	Amorphous - not refined							
	210								
	220								
	230								
	240								
	250								
[VO(L^3)(OMe)(MeOH)] (**7**)	30	8.914	8.2704(15)	11.375(3)	16.122(3)	90	95.543(13)	90	1509.6(5)
	40	8.548	8.2766(15)	11.403(3)	16.135(3)	90	95.515(13)	90	1515.7(5)
	50	8.767	8.2708(16)	11.400(3)	16.131(3)	90	95.456(14)	90	1514.1(6)
	60	9.064	8.2776(18)	11.424(3)	16.149(4)	90	95.411(16)	90	1520.3(6)
	70	5.237	14.513(3)	12.703(2)	7.0590(10)	90	92.057(9)	90	1300.5(4)
	80	4.857	14.527(3)	12.713(2)	7.0686(9)	90	92.043(8)	90	1304.6(4)
	90	4.950	14.541(3)	12.731(2)	7.0782(10)	90	92.034(8)	90	1309.5(4)
	100	5.002	14.532(3)	12.726(3)	7.0829(10)	90	92.019(9)	90	1309.1(4)
	110	4.924	14.534(4)	12.743(3)	7.0903(11)	90	91.995(9)	90	1312.4(5)
	120	4.902	14.531(3)	12.743(3)	7.0979(10)	90	91.968(9)	90	1313.5(5)
	130	9.048	14.81(4)	12.83(4)	7.154(16)	90	92.21(11)	90	1359(6)
	140	7.352	15.35(18)	12.93(15)	7.21(7)	90	92.0(3)	90	1430(30)
	150	4.937	15.43(12)	12.62(8)	6.81(5)	90	92.1(3)	90	1324(16)
	160	4.158	15.4(2)	12.80(19)	6.52(11)	90	94.0(2)	90	1280(40)
	170	4.265	14.98(13)	12.59(8)	6.38(6)	90	93.5(2)	90	1202(17)
	180	4.161	15.56(17)	13.00(13)	6.60(8)	90	93.5(2)	90	1330(30)
	190	4.082	15.2(2)	13.01(18)	6.48(9)	90	93.3(2)	90	1280(30)
	200	4.265	15.77(16)	13.07(12)	6.63(7)	90	93.8(2)	90	1360(20)
	210	4.210	15.3(2)	13.17(16)	6.52(9)	90	92.81(18)	90	1310(30)
	220	4.288	15.8(3)	13.4(2)	6.69(14)	90	93.4(2)	90	1410(50)
	230	4.271	15.70(15)	13.06(10)	6.65(7)	90	93.7(2)	90	1360(20)
	240	4.306	15.4(2)	12.71(18)	6.58(8)	90	94.1(3)	90	1290(30)
	250	4.222	15.0(3)	12.8(2)	6.41(11)	90	93.6(2)	90	1230(40)

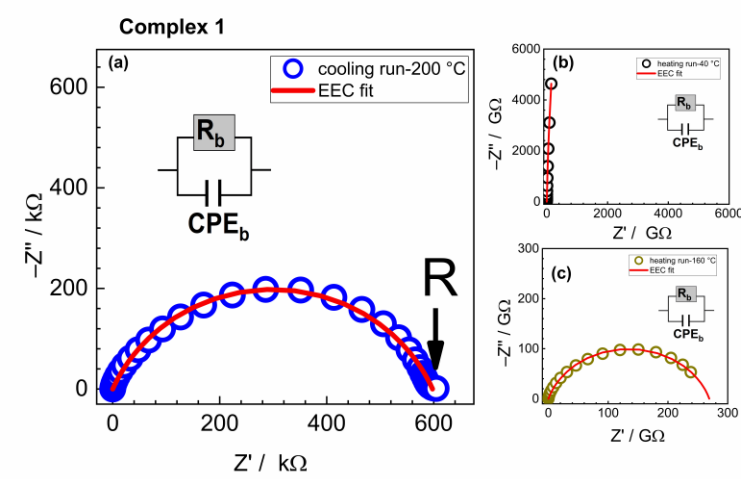

Fig S35.: Complex impedance spectra for **complex 1** at various temperatures in heating/cooling run. The coloured open circles denote experimental values, whereas the solid red line corresponds to the best fit. The corresponding equivalent circuit model is composed of parallel combinations of the resistor (R) and the constant-phase element (CPE), used for fitting the data of individual spectra.

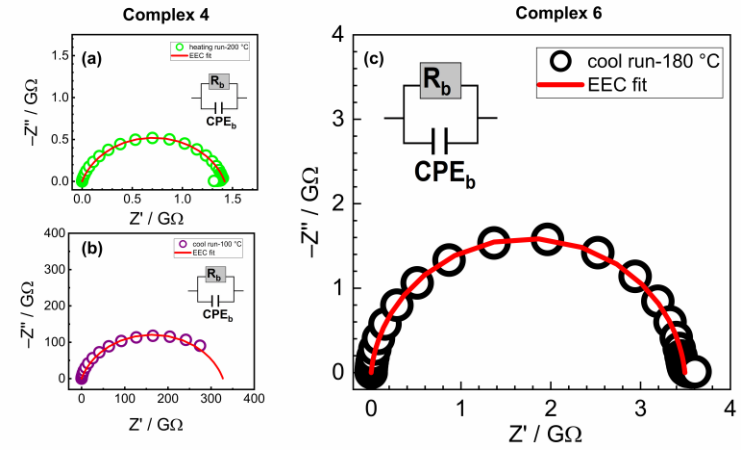

Fig S36. Complex impedance spectra for **complex 4** (a,b) and **complex 6** (c), at various temperatures in heating/cooling run. The coloured open circles denote experimental values, whereas the solid red line corresponds to the best fit. The corresponding equivalent circuit model is composed of parallel combinations of the resistor (R) and the constant-phase element (CPE), used for fitting the data of individual spectra.

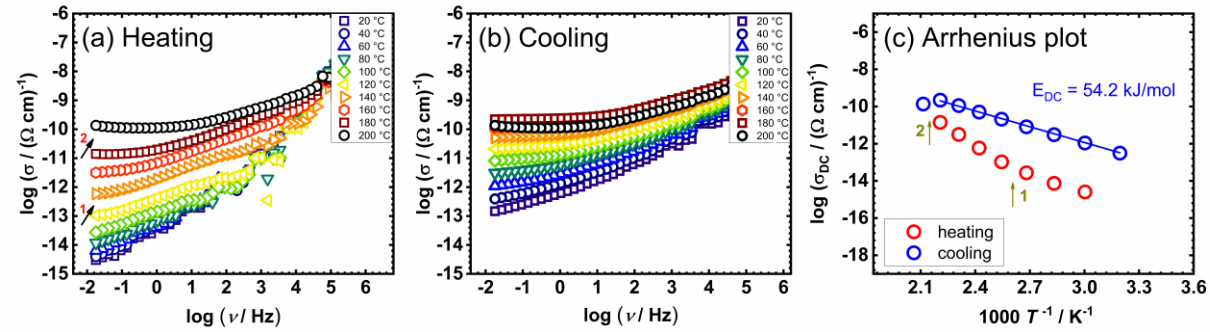

Figure S37. Conductivity spectra for mononuclear VO(L^1)(OMe)(MeOH)] sample (complex **2**) in heating (a) and cooling (b) runs, and (c) temperature dependence of DC conductivity (log(σ_{DC}) vs. 1000/T) for both runs (red circle—heating, blue circle—cooling).

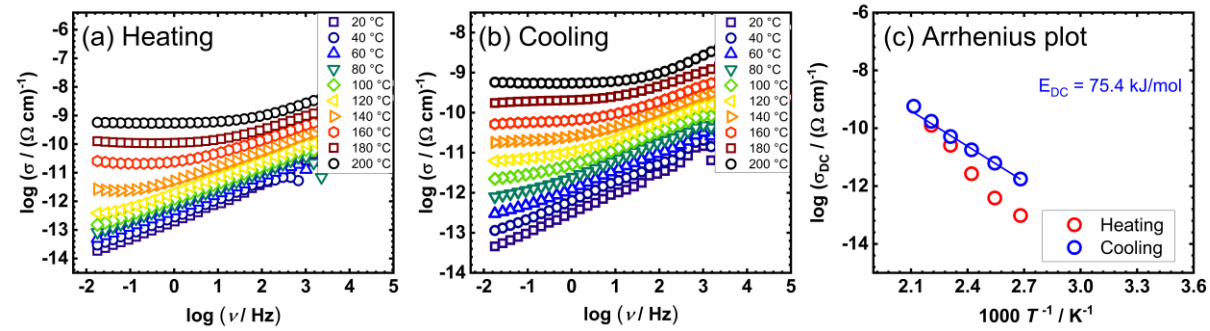

Figure S38. Conductivity spectra for mononuclear [$VO_2(HL^2)$] sample (complex **4**) in heating (a) and cooling (b) runs, and (c) temperature dependence of DC conductivity (log(σ_{DC}) vs. 1000/T) for both runs (red circle—heating, blue circle—cooling).

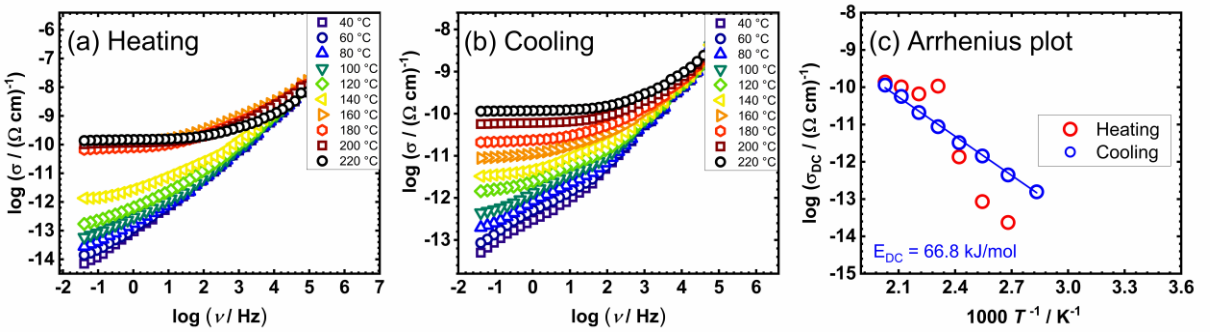

Figure S39. Conductivity spectra for mononuclear [VO(L^3)(OMe)(MeOH)] sample (complex **7**) in heating (a) and cooling (b) runs, and (c) temperature dependence of DC conductivity (log(σ_{DC}) vs. 1000/T) for both runs (red circle—heating, blue circle—cooling).